Poleward coastal jets induced by westerlies in the Bay of Biscay

Francois Batifoulier,[1,2] Pascal Lazure,[1] and Philippe Bonneton[2]

Received 7 October 2011; revised 10 January 2012; accepted 13 January 2012; published 16 March 2012.

[1] Two hydrodynamic surveys based on acoustic Doppler current profiler (ADCP) and drift buoys measurements taken in summer 2008 and 2009 revealed poleward coastal jets of up to 32 cm s^{-1} that lasted up to 22 d along the Aquitaine shelf in the southeastern area of the Bay of Biscay. A strong increase in bottom temperature was associated with these currents, up to 4°C in 5 d at 54 m depth. These observations occurred after a few days of westerlies, cross-shore winds which were thought to have only a limited impact on longshore circulation. Here, the MARS3D hydrodynamic model was used with a schematic bathymetry of the southeastern area of the Bay of Biscay to reproduce and analyze these coastal jets. Simulations revealed that the triggering mechanism of the poleward currents is unequivocally due to downwelling circulation induced along the Spanish coast. This downwelling induces an external longshore pressure gradient which generates a high-speed coastal-trapped wave that propagates along the French coast with a phase velocity of about 3 to 4 m s^{-1} and an internal baroclinic Kelvin wave with a phase velocity of about 1 m s^{-1}. A sensitivity study of the role of stratification conditions, wind strength and duration was then carried out to determine the periods that are the most sensitive to this wind-induced circulation.

Citation: Batifoulier, F., P. Lazure, and P. Bonneton (2012), Poleward coastal jets induced by westerlies in the Bay of Biscay, *J. Geophys. Res.*, *117*, C03023, doi:10.1029/2011JC007658.

1. Introduction

[2] The Bay of Biscay is located midway between France and Spain (Figure 1). Our study focuses on the southeastern area of the Bay of Biscay, which is shaped like a right angle made up of the Aquitaine coast (France) oriented along a near-perfect north-south axis and the Basque Country coast (Spain) oriented on an east-west axis. The width of the Aquitaine shelf tapers from 170 km off the Gironde River estuary to 30 km off the Basque Country coast. Off the shelf, the continental slope extends to the "Plateau des Landes" with a depth of between 1000 and 2000 m and extends 150 km westward to the abyssal plain. The Aquitaine shelf is cut by the Capbreton canyon whose head reaches the Aquitaine coast. Along Spanish coast, the continental shelf is particularly narrow (30 km wide); its depth reaches 160 m at the shelf break and it extends to a steep slope down to the abyssal plain.

[3] As this region is located at the midlatitudes, winds are variable throughout the year, but show seasonal patterns. Winds have a southwesterly direction in autumn and winter and a northwesterly direction in spring and summer, although interannual variability is great [*Lavin et al.*, 2006].

[4] Several observations of poleward currents have been reported in the Bay of Biscay during different seasons. It has long been known that the circulation along the western and northern coast of the Iberian Peninsula is subject to these poleward currents [*Relvas et al.*, 2007]. In autumn and winter, a warm, saline poleward-flowing slope current that originates on the Portuguese coasts enters the Bay of Biscay along the northern Spanish coast as far as the Cantabrian Sea [*Frouin et al.*, 1990; *Pingree and Le Cann*, 1992; *Relvas et al.*, 2007]. This mesoscale phenomenon called "Navidad" is located above the shelf break. Its easternmost extension as far as the Aquitaine shelf break has been demonstrated using drifted buoy and satellite SST images [*Le Cann and Serpette*, 2009]. However, its extension on the French and Spanish shelves has never been measured. Along the French coast, *Lazure et al.* [2008] described a poleward current over the Armorican shelf (north of the Aquitaine shelf, see Figure 1) with an average velocity of about 10 cm s^{-1} (with burst of 20 cm s^{-1}) in autumn. To date, no summer observations of poleward currents over the shelf have been reported in the southeastern area of the Bay of Biscay or, more generally, along the northern Spanish coast.

[5] The hydrodynamics of the southeastern area of the Bay of Biscay are poorly known and in situ long-term observations are still lacking. On the French continental shelf, hydrodynamics are governed by wind and density currents. Tidal currents are relatively weak, lower than 15 cm s^{-1} (except close to the coast) [*Le Cann*, 1990]. These weak tidal currents promote strong vertical stratification. Warm surface water is usually observed in this area during summer [*Koutsikopoulos and Le Cann*, 1996] and is attributed to weak summer winds. Salinity patterns are influenced

[1]IFREMER, Centre de Brest, Plouzané, France.
[2]UMR CNRS EPOC 5805, Université de Bordeaux I, Talence, France.

0148-0227/12/2011JC007658

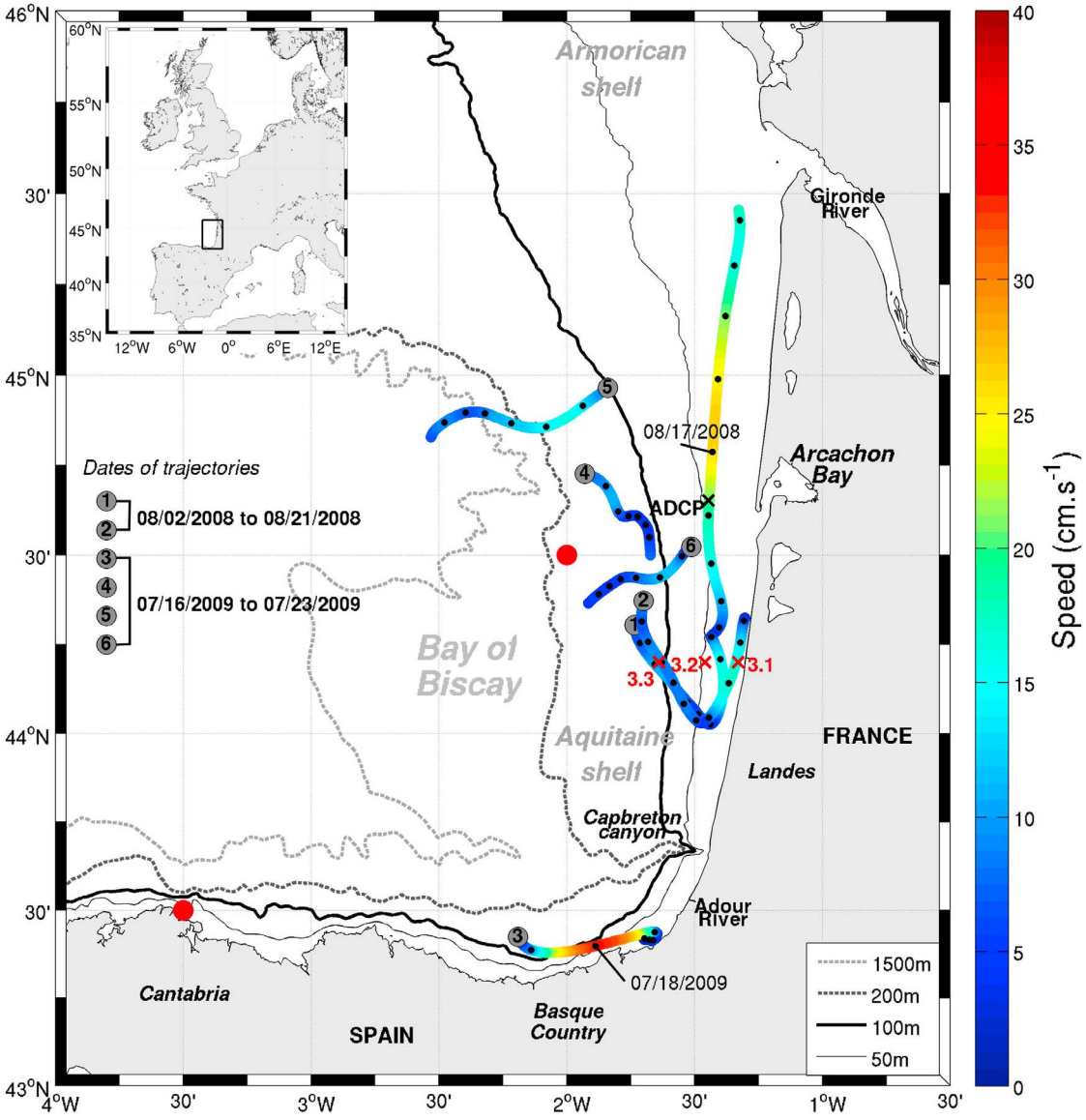

Figure 1. Map of the Bay of Biscay and tide filtered buoy trajectories in 2008 (Buoys 1 and 2) and 2009 (Buoys 3 to 6). Dots on trajectories are separated by an interval of 1 d.

by two major rivers, the Gironde River (100 km north of Arcachon Bay, whose mean annual runoffs are 885 $m^3 s^{-1}$) and the Adour River (120 km south of Arcachon Bay; whose mean annual runoffs are 315 $m^3 s^{-1}$). The dynamics of these river plumes are influenced by wind regimes and show high seasonal variability [*Puillat et al.*, 2004; *Ferrer et al.*, 2009; *Petus et al.*, 2010].

[6] From spring to autumn, prevailing northwesterly winds are able to induce transient upwellings along the Landes coast which are visible on satellite images [*Froidefond et al.*, 1996]. Numerical barotropic simulations [*Pingree and Le Cann*, 1989] show that on the Aquitaine shelf, the resulting wind-driven currents are typically of about 10 cm s^{-1} and locally up to 20 cm s^{-1}. Northwesterly and westerly winds cause southward currents. The southwesterly and southerly winds reverse the general circulation toward the northwest. Lagrangian drifter trajectories collected from 1992 to 2009 show that residual currents on the Aquitaine shelf are poleward in the spring, about 5 cm s^{-1}, and equatorward in the summer, about 2 cm s^{-1} [*Charria et al.*, 2011].

[7] Along the Spanish shelf, recent investigations provide a better description of seasonal patterns on the Basque Country coast [*Valencia et al.*, 2004]. Offshore, during spring and summer, moderate northerly and easterly winds induce alternating southward and westward circulation and upwelling events along the Spanish coast. These factors maintain the stratification and the vertical stability of the water column. During autumn and winter, strong southerly and westerly winds prevail, inducing eastward and northward currents and the dominance of downwelling in the southeastern area of the Bay of Biscay.

[8] Here, we present recent measurements taken in the summer that reveal intense poleward coastal currents on the French Aquitaine shelf of up to 32 cm s^{-1} and nearly homogeneous from the surface to the bottom. They generally lasted a few days, but could last up to 22 d. A recent study showed that these currents may transport harmful *Dinophysis* spp. blooms from the Basque Country and south of the Aquitaine shelf to the Arcachon Bay [*Batifoulier et al.*, 2011]. It has been demonstrated that the trigger consists of several days of westerlies which are cross-shore winds along the Aquitaine coast. This observation deserves further investigation because it is known that cross-shore winds have only a limited impact on longshore circulation; the present paper focuses on the mechanism that triggers these currents.

[9] In section 2, we describe two periods of observation of poleward current events in 2008 and 2009 and the meteorological and hydrological conditions associated with these events. Then, in section 3, a hydrodynamic 3-D model is used to schematically simulate and analyze the mechanism that gives rise to this poleward current and its fate. The sensitivities of hydrometeorological parameters (wind and water column stratification) are then explored.

2. Observations

[10] Here, we describe two acoustic Doppler current profiler (ADCP) data sets in 2008 and 2009 and the associated meteorological conditions. Drift buoys trajectories available during these measurements help to understand the offshore extension of this current on the Aquitaine shelf.

2.1. Field Data

[11] Coastal currents were measured with an ADCP (RDI 300 KHz) moored, bottom-mounted, offshore Arcachon Bay (44.65°N, 1.45°W; see location in Figure 1) at a depth of 54 m from 9 July to 25 August 2008 and a slightly inshore at a depth of 51 m from 18 May to 13 August 2009. Current velocities were recorded at 5 min intervals with a bin size of 1.5 in 2008, and at 10 min intervals with a bin size of 1 m in 2009. In addition to current measurements, the ADCP also measured bottom temperature and pressure.

[12] A Demerliac filter [*Demerliac*, 1974] was used to remove the tidal signal from current and pressure data. Data corresponding to the first 6 m below the surface (detected with the pressure sensor) were considered too noisy to be properly analyzed.

[13] In August 2008, the trajectories of two satellite-tracked drift buoys drogued at 15 m were available (Buoys 1 and 2 in Figure 1). In July 2009, four trajectories of satellite-tracked buoys drogued at a depth of 15 m were used (Buoys 3 to 6 in Figure 1).

[14] 2009 ADCP and buoys data were partially presented by *Batifoulier et al.* [2011]. Wind data were extracted from the results of Meteo-France's atmospheric ARPEGE model. It provides wind fields four times a day with a 0.5° resolution in longitude and latitude (i.e., 55.6 km).

[15] A few CTD casts were performed in July and August 2008 during the ARCADINO surveys along a network of stations located on the Aquitaine shelf. The CTD instrument was a SBE 25 SEALOGGER CTD.

[16] The Adour River flow was provided by the French Freshwaters Office database (http://www.hydro.eaufrance.fr/). The time series used were based on daily measurements.

2.2. The August 2008 Event

2.2.1. Meteorological and Hydrological Conditions

[17] Figure 2a gives the progressive vector diagram of wind stress recorded during the 2008 ADCP measurements. Winds close to the ADCP location (44.5°N, 2°W) were northerly until 31 July and then became westerly until the end of the record except for short weak northerly events on 5 and 6 August. Two events of westerlies were observed. The first one was moderate and occurred from 7 August with winds of up to 8.5 m s^{-1} to 8 August when winds turned from the northwest (with an eastward component of 6 to 8.5 m s^{-1} for 24 h). The second one was more intense and lasted from 12 to 13 August with westerlies of up to 12.5 m s^{-1} (with an eastward component of 7 to 12.5 m s^{-1} for 36 h). Moderate westerlies then blew until the end of the record.

[18] Winds on the Spanish coast (43.5°N, 3°W) are similar to those on the Aquitaine coast. During the event of intense westerlies from the 12 to 13 August on the Aquitaine coast, winds on the Spanish coast were from the WSW and also strong.

[19] The Adour flow was moderate during the poleward currents: it was lower than 150 m^3 s^{-1} for 3 weeks (starting 19 July) which is about half of its annual mean value.

2.2.2. Current Measurements

[20] Figure 3 shows ADCP measurements from 11 July to 20 August 2008. Cross-shore currents (Figure 3a) were rather weak during the whole recording period; they were maximum at the surface, between −12 cm s^{-1} (westward) and 12 cm s^{-1} (eastward). From 19 to 24 July, longshore currents (Figure 3b) were negative throughout the water column (southward), and stronger at the surface, up to −16 cm s^{-1}. During the same period, cross-shore bottom velocities were positive toward the coast (Figure 3d) and the sea surface height (SSH) decreased (Figure 3c). These observations are typical of an upwelling episode and occurred during northerlies (Figure 2a), upwelling favorable winds. After 24 July and until 7 August, currents weakened at the bottom but surface currents continued to flow toward the south. As of 7 August, winds turned eastward (Figure 2a), surface currents were oriented toward the southwest. Under the surface, longshore currents turned poleward, but remained weak. The SSH started to rise with the westerlies. As of 14 August, after the second (much stronger) event of westerlies (Figure 2a), strong northward currents were recorded over the entire water column until the end of the recording period. These poleward currents reached 32 cm s^{-1} near the surface. These intense currents were preceded by southeasterly surface currents and offshore bottom velocities (Figure 3d).

[21] The bottom temperature (Figure 3c) was nearly constant at about 13°C from the beginning of the record until 16 August. As of 16 August, it rose sharply from 13°C to 15°C and up to 17°C on 22 August at the end of the record. The temperature oscillated at the M2 (principal lunar semidiurnal tidal component) tidal frequency; the temperature variation at the bottom reached 2.4°C between low and

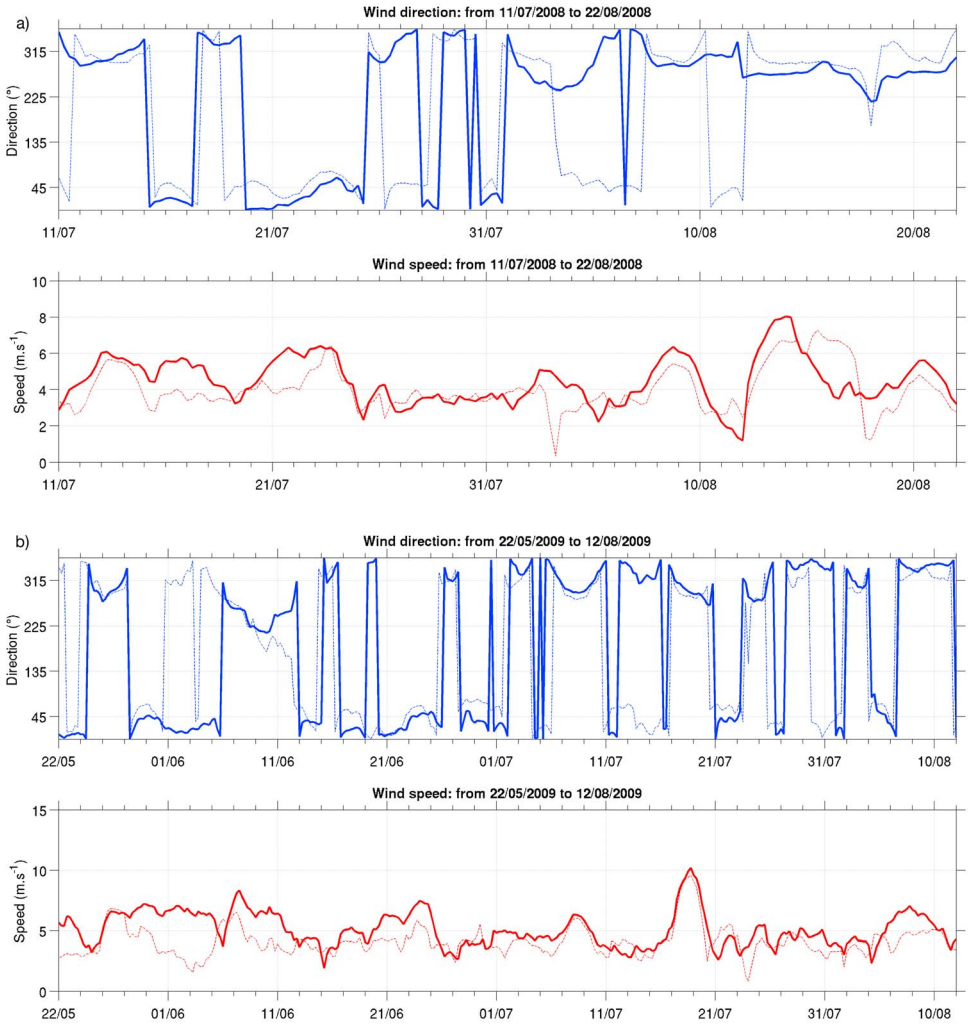

Figure 2. Time series of wind direction and speed (a) from 11 July 2008 to 20 August 2008 and (b) from 22 May 2009 to 8 December 2009, analyzed at 44.5°N, 2°W in solid line and at 43.5°N, 3°W in dashed line. See red dots in Figure 1 for locations of wind data from the ARPEGE model.

high tide on 21 August. The increase in SSH, offshore bottom velocities, bottom temperature and the poleward current at all water depths is typical of a downwelling episode despite the fact that they occurred during westerlies which are not downwelling favorable winds.

[22] The depth of the bottom boundary layer can be estimated from Figures 3a and 3b. It was estimated at about 30 m, since the longshore current was sheared at this depth and nearly homogenous above.

[23] Two satellite-tracked drifters were deployed on the Aquitaine shelf during the ADCP measurements; their trajectories are shown in Figure 1 (Buoys 1 and 2). Both buoys headed southeast until 7 August. The speed of the buoys during their southward displacement was about 10 cm s^{-1}. On 7 August, the buoys abruptly changed direction with the onset of westerlies and started to drift poleward along the 60 m isobath with a speed increased up to 20 cm s^{-1}. From 10 August, the speed of the buoys decreased, Buoy 2 ran aground on 12 August. Buoy 1 resumed its poleward progression, from 11 to 20 August, it covered about 270 km with speeds up to 27 cm s^{-1} and then ran aground. On 15 August, the buoy passed right over the moored ADCP. Speed measured by the ADCP (at 15 m above the sea surface) and the buoy speed were quite similar: 18 cm s^{-1} according to the ADCP and 21 cm s^{-1} according to the buoy.

[24] The maximum buoy velocity was reached on 16 August (27 cm s^{-1}), while the maximum ADCP velocity was reached on 17 August (32 cm s^{-1}). This delay will be discussed below.

2.3. The July 2009 Event

2.3.1. Meteorological and Hydrological Conditions

[25] The progressive vector diagram of wind stress close to the ADCP location (44.5°N, 2°W) during the 2009 event is shown in Figure 2b. Up until 16 July winds were mainly northerly except for an event of west-southwesterly winds from 5 to 7 June with intensities of up to 10.7 m s^{-1}

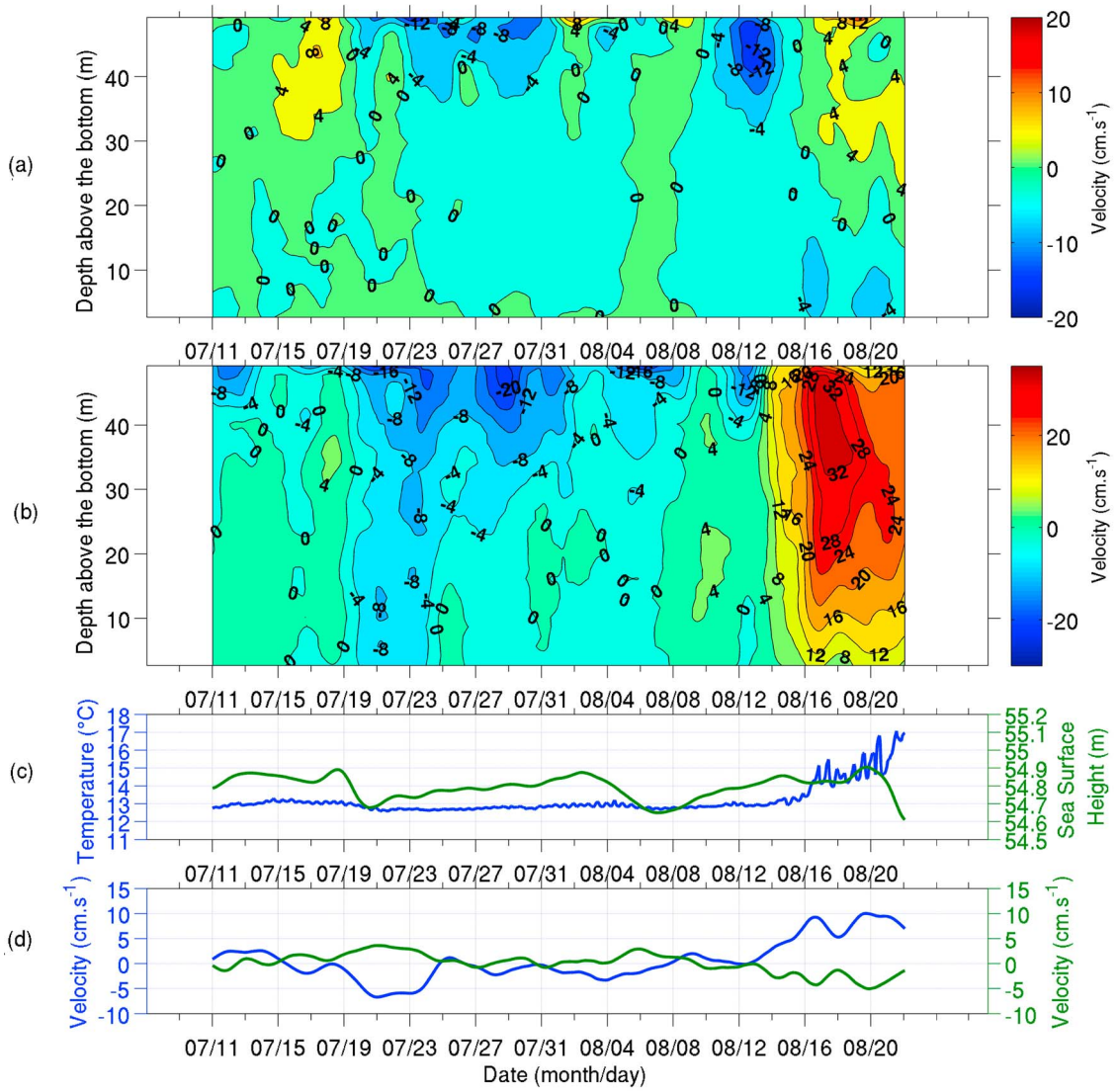

Figure 3. Acoustic Doppler current profiler (ADCP)2008 data: (a) cross-shore velocity, U; (b) longshore velocity, V; (c), bottom temperature (54 m depth) and sea surface height (SSH); and (d) cross-shore (in green) and longshore (in blue) bottom velocities.

(eastward component from 7 m s^{-1} to 10.5 m s^{-1} for 42 h) followed by short bursts, also from the west-southwest, on 9 and 10 June. Then winds were weak until 15 June when northerlies blew again. From 6 to 8 July, weak winds blew from the west-northwest with a maximum of 7 m s^{-1} for the eastward component. Strong west-northwesterly winds of up to 14.3 m s^{-1} (east-west component from 7 m s^{-1} to 12.3 m s^{-1} for 54 h) blew from 16 to 19 July and then weak northerlies blew until the end of the record.

[26] Winds on the Spanish coast (43.5°N, 3°W) show that the first event of westerlies on the Aquitaine coast from 5 to 7 June was much weaker. However, the second event from the west-northwest from the 16 to 19 July did also occur on the Spanish coast.

[27] Adour flow was moderate during the poleward currents event: it was lower than 150 m^3 s^{-1} for more than 2 weeks (since 1 July).

2.3.2. Current Measurements

[28] Current measurements taken from 22 May to 12 August 2009 are shown in Figure 4. Cross-shore currents (Figure 4a) were quite low during the whole recording period, between −8 and 12 cm s^{-1} and showed high temporal variability.

[29] From 25 May to 5 June, southward surface currents were associated with northerlies (Figure 2b). Cross-shore currents were offshore at the surface (beyond the first 6 m that were ignored) and onshore below the surface. The SSH decreased slowly during this period, the bottom temperature (Figure 4c) was constant at about 12°C.

[30] From 16 to 25 June, longshore currents were mainly negative (southward) and stronger at the surface, up to −20 cm s^{-1}. These southward currents were associated with northerlies that had been blowing since 15 June (Figure 2b). A countercurrent appeared at 30 m from the bottom on 25 June, but velocities remained weak. Until

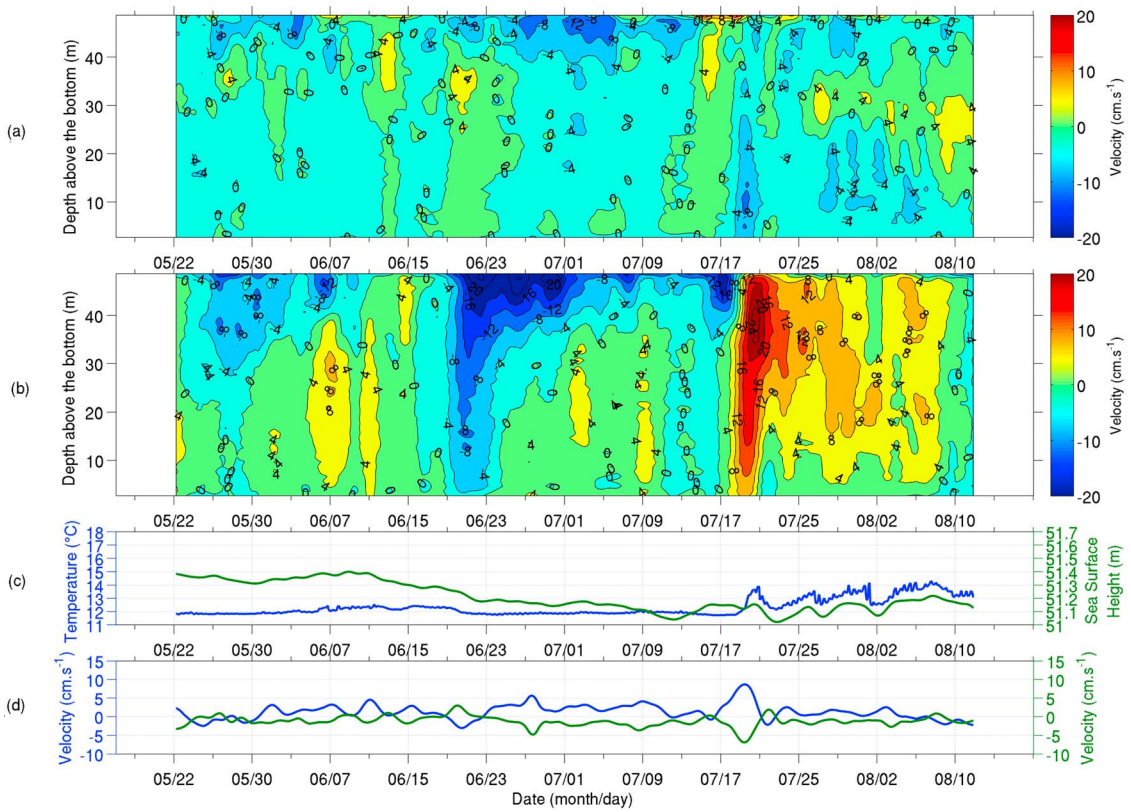

Figure 4. ADCP 2009 data: (a) cross-shore velocity, U; (b) longshore velocity, V; (c) bottom temperature (51 m depth) and SSH; and (d) bottom velocities, cross-shore (in green) and longshore (in blue).

11 July cross-shore currents were negative in the surface layer and weakly positive below. Bottom temperature decreased slightly to 12°C on 19 June. The SSH decreased monotonically as of 11 June when northerlies set up. These observations are typical of an upwelling episode.

[31] On 17 July, strong southeastward surface currents of up to 16 cm s^{-1} were associated with intense west-northwesterlies (Figure 2b). At the same time, poleward currents set up under the surface to the bottom (Figures 4b and 4d). On 19 July, currents were poleward in the entire water column with a maximum velocity of 24 cm s^{-1}. Cross-shore currents that were onshore before 17 July turned offshore near the bottom (Figure 4d). The increase in poleward velocities and offshore bottom currents was associated with a sharp increase in temperature from 12°C to 14°C on 19 July. As in August 2008, the offshore bottom velocities, the rise of bottom temperature and the poleward current at all depths are typical of a downwelling episode. However, they occurred during west-northwesterlies which are not downwelling favorable.

[32] On 22 July, the wind turned southward until the end of the record (Figure 2b), poleward currents weakened and the temperature stopped rising and then decreased. However, up until the end of the recording period, significant northward currents were recorded (up to 12 cm s^{-1}) in the entire water column with different maximums. These maximums also occurred with increases in temperature and SSH. On 10 August, the poleward flow stopped 22 d after the burst of westerlies.

[33] Four buoys were launched on the shelf before the strong currents measured in late July 2009; their trajectories and speed are shown in Figure 1 (Buoys 3 to 6). Buoy 3 in the south near the Basque Country coast was caught in an intense current from 17 to 19 July that went along the coast at speeds of up to 33 cm s^{-1} (18 August 2009, 01:45) and then ran aground. In the north, the longshore component at 15 m below sea level (depth of the buoy drogue) measured by the moored ADCP, reached a maximum velocity of 25 cm s^{-1} on 20 July 2009 at 12:30, about 59 h after the buoy had reached its maximum velocity.

[34] The three buoys offshore Arcachon Bay had different behaviors. Two of them moved slowly offshore (Buoys 5 and 6), while the third one went toward the south (Buoy 4). These buoys were not caught up in the poleward current; this shows that the poleward current width was limited to a jet close to the coast (within 30 km) that did not reach the 100 m isobath.

2.4. Summary of Observations, Preliminary Interpretations and Simulation Strategy

[35] The two episodes of poleward jets occurred during mean periods of upwelling favorable winds. A few days of westerlies (2008) or west-northwesterly winds (2009) apparently modified the mean circulation, which passed from equatorward to poleward. Circulation during both episodes was typical of a downwelling episode, although the winds were not downwelling favorable. Unfortunately, the ADCP record ended during the event in 2008; in 2009, the circulation remained poleward even when the winds

returned to their northerly direction. Interestingly, theoretical work, including barotropic simulations [*Pingree and Le Cann*, 1989] and schematic simulations [*Tilburg*, 2003], has shown that it is unlikely that cross-shore winds (westerlies) could trigger a noticeable poleward current such as the ones described above. We nevertheless explored the role of this type of forcing in section 3.

[36] As enumerated by *Gill* [1982], at least three mechanisms are able to induce poleward flow along an east-to-west oriented coast.

[37] First, poleward currents can be generated by density gradients from high river outflow. However, it is unlikely that in the summer, buoyancy inputs by a local river are dominant. No dramatic changes in river runoff were associated with the observed changes in longshore currents. Salinity profiles during ARCADINO surveys in 2008 (not shown) showed weak salinity stratification (surface and bottom waters of 35.1 and 35.5 psu, respectively) at station 3.2 (44.2°N, 1.46°W) (at 50 m depth) associated with river plumes and this stratification was restricted to the surface layer. Moreover, the vertical structure of the poleward current extended through most of the water column, whereas poleward currents associated with a river plume, when it is detached from the bottom, are restricted to the surface layer [*Garvine*, 1987; *Yankovsky and Chapman*, 1997].

[38] Second, upwelling relaxation may be an explanation because our observations occur after upwelling periods. These phenomena have been widely studied along the coast of California during the last decades. *Melton et al.* [2009] and *Pringle and Dever* [2009] recently showed that upwelling relaxation could be induced by wind relaxation or reversal during the upwelling season and that longshore wind gradients and longshore bathymetric variations are also able to trigger poleward jets. However, the Bay of Biscay is located too far north to clearly identify a season of permanent upwelling. For this reason, we first assume that there is no need for upwelling to occur prior to the setup of a poleward current as observed.

[39] Third, the influence of remote winds is the most plausible mechanism at work during the observed events. On the basis of several studies along the Californian coast cited by *Pringle and Dever* [2009], it has been shown that local currents can be better explained by remote winds blowing at 200–300 km to the south, upstream from the direction of propagation of the Kelvin wave. At 150 km south of our observations, the Spanish coast orientation changes dramatically. As stated recently by *Sanay et al.* [2008], following previous studies [*Crépon and Richez*, 1982], the effects of coastline variation are similar to the effects caused by alongshelf changes in wind forcing. In that respect, westerlies are perfect downwelling favorable winds for the Spanish Atlantic coast. In the absence of any observations of coastal currents or hydrology along this coast, we based our analysis of the dynamics along the Spanish coast on the theoretical or schematic simulations of downwelling circulation given by *Allen and Newberger* [1996] and *Austin and Lentz* [2002].

[40] Our strategy therefore focuses on the effect of the change in the coastline. To reproduce and analyze the triggering mechanism that gives rise to this current, we used a process-oriented modeling approach. We considered two coastline configurations: a coastline that forms a southeast-lying right angle similar to that formed by the Spanish Basque Country and the French Aquitaine coasts and a simple straight coastline. Sensitivities of wind intensity, wind duration, stratification gradient and stratification depth were explored. Further investigations were performed to understand the reason why the west-southwesterly winds from 5 to 7 June 2009 did not trigger a poleward current.

3. Modeling Simulations

3.1. Model Setup

[41] The MARS3D hydrodynamic model [*Lazure and Dumas*, 2008] was used in a schematic configuration. This 3-D model is a classical free surface model with generalized sigma vertical coordinates. The one equation turbulence closure scheme of *Gaspar et al.* [1990] was used in all simulations. The lateral eddy viscosity was 0.63 $m^2\ s^{-1}$.

[42] Two schematic bathymetries were used. The Bay of Biscay was represented by a rectangle with one side (representing the Spanish coast) 450 km long and one side 600 km long (representing the French Aquitaine coast). The bathymetry was set up to represent the main characteristics on both sides of the southeast-lying right angle coastline. The French shelf was represented with the following characteristics: at 44°N the shelf has a width of 58 km and a slope of 0.22% running from 10 m from the coast to 160 m at the shelf break. The modeled Spanish shelf had a width of 30 km with a slope of 0.45% running from 10 m from the coast to 160 m at the shelf break. The distance from the shelf break to the abyssal plain is represented on both sides of the right angle by a slope of 55 m km^{-1} with a width of 34 km, running from 160 m to 2000 m. Far from the area studied, the two remaining sides of the rectangle close the domain on the western and northern sides. The right angle bathymetry was modeled as close as possible to the real bathymetry; the geographical coordinates used in the study were based on the real coordinates. In our configuration, the southeast-lying right angle had the following coordinates: 42.9 to 48.8°N and −7 to −0.7°W. The second schematic bathymetry used was the same as the first one, but the Spanish coast and the corner were removed: only one straight side north of latitude 43.9°N, which represents the French coastline, was kept. In this straight coastline bathymetry, boundaries were left open. Both bathymetries had a horizontal grid size of 2 km and 50 vertical sigma levels were considered with a higher resolution near the surface. All simulations started from a state of rest with a horizontally uniform density field.

[43] The basic case (BC) simulation lasted 14 d. The forcing consists in 3 d of spatially uniform westerlies of 10 m s^{-1} (i.e., wind stress of 0.2 $N.m^{-2}$). The initial stratification consisted of three layers: a surface homogeneous layer of 30 m with a surface temperature (Ts) at 22°C, a thermocline from 30 m to 40 m with a temperature gradient running from 22°C to 12°C and a bottom layer from 40 m to the bottom at 12°C. This stratification represents the typically strong summer stratification in the southeastern area of the Bay of Biscay. Salinity gradients were not considered in the BC; density therefore depended only on temperature. The time step varied from 40 to 200 s.

[44] We performed 50 different simulations in which we varied the basic parameters of the system: the magnitude,

Table 1. Description of Simulations

Run	Bathymetry	Wind Intensity (m s^{-1})/ Number of Days of Wind	Wind Direction	Depth (m)/Temperature (°C) of First Layer	Depth of Thermocline (m)/ Bottom Temperature (°C)
BC	1	10/3	270	30/ 22	10/12
BCh	1	10/3	270	30/12	10/12
3–10	1	10/3	0:45:360	30/22	10/12
SC1	2	10/3	270	30/22	10/12
SC2	2	X	X	30/22	10/12
SC3	2	X	X	30/22	10/12
14–21	1	(2, 4, 6, 8, 10, 12, 14, 16)/3	270	30/22	10/12
22–26	1	10/(0.5, 1, 2, 3, 6)	270	30/22	10/12
27–38	1	10/3	270	30/(12, 13, 14, 15, 16, 17, 18, 19, 20, 21, 22, 23)	10/12
39–44	1	10/3	270	(7.5, 10, 15, 20, 30, 40)/22	(2.5, 3.33, 5, 6.66, 10, 13.33)/12
45–51	1	10/3	270	Realistic thermoclines and haloclines	

direction and duration of the wind stress, the depth of the thermocline and the temperature gradient in the thermocline. The right angle configuration was used in all these simulations. A list of the simulations performed is given in Table 1. The BCh simulation is the same simulation as the BC, but without stratification. Wind direction varied at all angles (N, NW, W, SW, S, SE, E, NE, runs 3 to 10, see Table 1). Wind magnitude varied from 2 to 16 m s^{-1} (i.e., wind stress from 0.008 to 0.512 N.m^{-2}, runs 14 to 21, see Table 1). Duration of the wind stress varied from one-half day to 6 days (runs 22 to 26, see Table 1). In all simulations, the wind was relaxed to zero abruptly within one time step. Temperature in the surface layer varied from 12 to 23°C (runs 27 to 38, see Table 1). Thickness of the surface layer varied from 7.5 to 40 m (runs 39 to 44, see Table 1); the thermocline thickness was always set as one third of the surface layer. Six additional simulations (runs 45 to 51) with realistic density conditions (in terms of salinity and temperature) in February, April, June, August, October and December were performed. Temperature and salinities were initialized with mean profiles on the Aquitaine shelf extracted from the monthly climatology Bobyclim (http://www.ifremer.fr/climatologie-gascogne). Wind duration and length was 3 d of 10 m s^{-1}.

[45] Three other simulations (run SC1 (where SC stands for Straight Coastline), SC2 and SC3; see Table 1) were conducted with the straight coastline bathymetry to test the response of the French coast only. In these simulations, a null velocity gradient was imposed at the open boundaries. In run SC1, the sea surface height (SSH) was set to zero on all open boundaries. Three days of westerlies of 10 m s^{-1} were imposed (as in the BC simulation). In run SC2, no wind was imposed. On the southern boundary (at latitude 43.9°N), SSH extracted from the BC simulation at the same latitude was imposed. Western and northern boundaries of the SSH were set to zero. The density field on the boundaries depended on the velocities in the grid cell found at the edge of the boundary. If velocity was positive toward the interior domain, the density field was set to the initial conditions. If velocity ran out of the domain, the density field was set to the density field in the preceding grid cell.

[46] In run SC3, only the density field extracted from the BC was imposed on the southern boundary. On the other boundaries, the density field was set as in run SC2. SSH was set to zero on all boundaries as in SC1.

3.2. Basic Case Experiment

[47] The basic simulation (BC) consists in 3 d of 10 m s^{-1} of westerlies with a water temperature vertical profile of 22°C in the first 30 m and a gradient down to 12°C at 40 m. Results are given in Figure 5. Depth-averaged current magnitudes, location of the front (intersection between the 17°C isotherm and the bottom) and SSH is given for different dates in Figure 5a. For clarity and to focus on the changes in magnitude, we do not give the velocity vectors, which are closely oriented along the isobaths in the poleward direction. Figure 5b shows a vertical transect of the Spanish coast at 2°W of the zonal velocities (positive when the current is eastward) and the superimposed isotherms (i.e., isopycnals when salinity is constant) and Figure 5c shows a vertical transect off the French Aquitaine coast at 44.5°N of the meridional velocities (positive when the current is northward) and superimposed isotherms. The wind was relaxed to zero after 3 d.

[48] Temporal trends in synthetic variables were also used to describe the BC experiment (Figure 6): Hp is the depth where the 17° isotherm intersects the bottom; Vmax, the maximum poleward velocities along each transect; SSH, the sea surface height on the different transects at the coast.

3.2.1. Along the Spanish Coast

[49] Along the Spanish coast, downwelling favorable winds first drive longshore transport close to the coast and an increase in SSH of up to 10 cm (see Figures 5a and 5b, t = 1.5 d). Onshore Ekman transport in the surface boundary layer deepens the pycnocline at the coast (Figures 5a and 5b, t = 1.5, 3.5 d), indicating that warm surface water plunges at the coast, creating a bottom front with a strong cross-shelf density gradient near the bottom. On day 3.5, SSH decreases when the wind stops blowing. A strong surface-intensified current develops above the front (see Figure 5b) with zonal velocities ranging from 40 cm s^{-1} to 60 cm s^{-1}. Then after the wind stops (Figures 5a and 5b, t = 5.5, 9.5, and 13.5 d), the pycnocline goes back up, the intensity of the current weakens and the SSH decreases to under 4 cm. A countercurrent develops between the front and the Spanish coast (Figure 5b, t = 5.5, 9.5, and 13.5 d). The front on the Spanish transect (2°W) deepens while the wind blows (3 d) to a maximum depth of 69.5 m (Hp2W BC, Figure 6a). Then the front retreats slowly until the end of the simulation. The maximum flow in the jet (Umax2W, Figure 6b) increases to a maximum of 80 cm s^{-1}. When the wind stops,

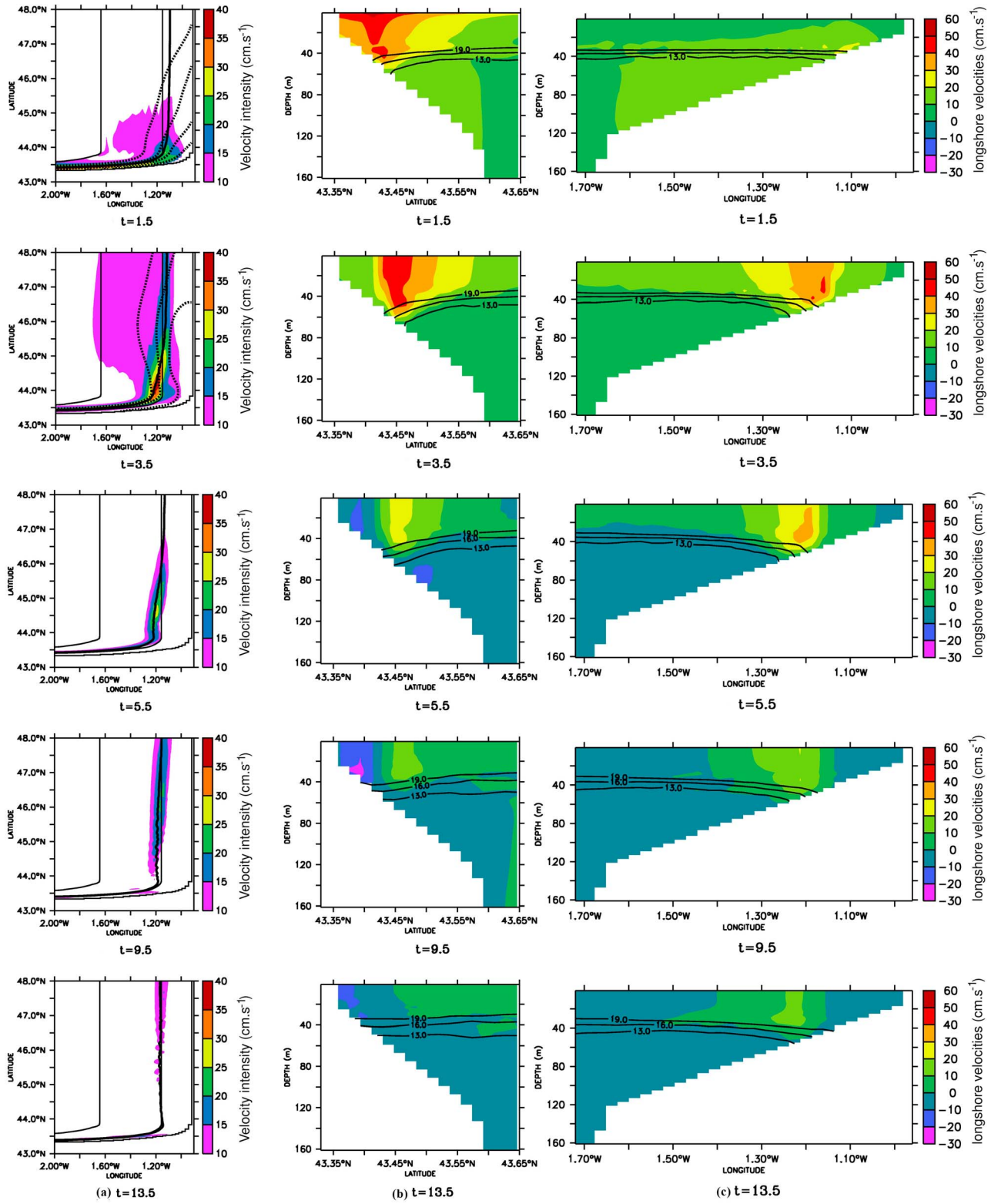

Figure 5. Results from the basic simulation (BC). (a) Depth-averaged velocities and location of the front (intersection between the isotherm 17°C and the bottom); solid lines: isobaths 0, 50, and 150; dashed lines: SSH isocontours from 4 cm to 10 cm in increments of 2 cm. (b) Vertical transect at 2°W of the zonal velocities and the superimposed isotemperature. (c) Vertical transect at 44.5°N of the meridional velocities and superimposed isotemperature for different times during simulation. Time is given in days.

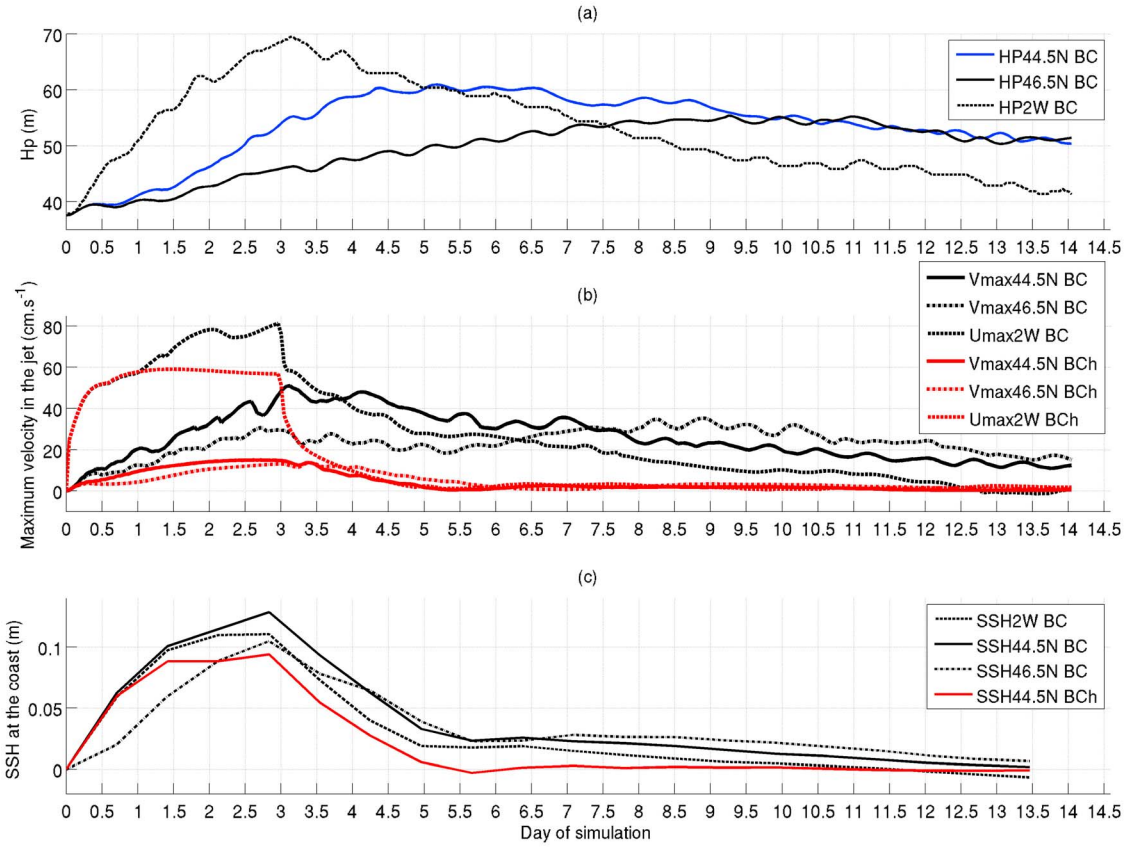

Figure 6. Time evolutions of (a) Hp, depth of the front; (b) maximum longshore barotropic velocities in the jet; and (c) SSH at the coast, subsampled each 17 h. BC, BC simulation; BCh, BCh simulation (see Table 1). Hp is defined as the depth where the 17° isotherm intersects the bottom. Hp2W BC, the 2°W section on the Spanish coast; Hp44N5 BC, section 44.5°N on the French coast; Hp46.5N, 46.5°N on the French coast; Vmax or Umax, maximum poleward velocities along each transect; SSH, sea surface height on the different transects at the coast.

the speed of the coastal current decreases quickly on the first day, more slowly thereafter and vanishes at the end of the simulation.

[50] The SSH at the coast at longitude 2°W (XE 2W BC, Figure 6c) increases quickly to its maximum value of 0.11 m after 3 d and then decreases until day 5, after which it remained lower than 0.02 m until the end of the simulation.

3.2.2. Along the French Coast

[51] At 1.5 d, from the Spanish coast to latitude 45°N, a poleward flow along the whole shelf set in (Figure 5a, t = 1.5). The transect at latitude 44.5°N (Figure 5c) shows that the flow over the shelf is weaker in the Ekman surface layer because the southward currents resulting from the westerlies counteract the mean poleward flow. The increase in SSH along the Spanish coast propagates along the French coast. At 3.5 d, the poleward flow spreads over the entire French shelf (Figure 5a). South of 44.5°N, SSH decreases, whereas north of 44.5°N, SSH continues to propagate. The front deepens and moves away from the coast (Figure 5c, t =3.5 d). At the same time, a poleward jet strengthens. This phenomenon involves the entire French shelf, although it is more pronounced in the south than in the north. Velocities in the jet along the French coast at latitude 44.5°N are about 20 cm s^{-1} to 50 cm s^{-1} lower than in the jet along the Spanish coast. At 5.5 d, the SSH decreases to less than 4 cm; the poleward flow on the entire shelf stops, but the poleward jet remains (Figure 5a, t=5.5 d). Currents between the jet and the coast are weak. The location of the maximum velocities moves north. At 9.5 d, the jet keeps on propagating northward (Figure 5a, t = 9.5 d). and at 13.5 d, it almost disappears (Figure 5a, t = 13.5 d). Behind the jet, velocities weaken and the isotherms return to their original values (Figure 5a, t = 9.5 d).

[52] The front on the French coast along the 44.5°N transect continues to deepen for 5 d even when the wind is relaxed (Figure 6a). It stays at about 60 m and then withdraws very slowly; at the end of the simulation, the front is still at 51 m (initially it was at 40 m). The deepening of the stratification is delayed in the 46.5°N transect; the maximum Hp is reached after 9 d (i.e., 6 d after the wind stops). The maximum velocity in the 44.5°N transect is 45 cm s^{-1} and is reached after 3 d and then decreases slowly (Figure 6b). The jet along the French coast lasts longer than the jet along the Spanish coast, even once the wind has stopped. On the 46.5°N transect, an initial maximum of 0.3 m s^{-1} is reached after 3 d, then the velocity decreases to 0.18 m s^{-1} on day 5 and rises again to 0.35 m s^{-1} on day 8; this second increase will be discussed further below.

[53] The SSH at the coast at the 44.5°N transect (XE 44N5 BC, Figure 6c) starts to increase after one-half day. The

maximum SSH (0.13 m) is reached after 3 d (before the wind stops). The SSH at the coast in the 46.5°N transect (XE 44N5 BC, Figure 6c) is delayed for about one-half day, a maximum of 0.11 m is also reached after 3 d. Once the wind stops, SSH on both transects drops almost instantaneously to 0.03 m and then decreases slowly for 5.5 d, after which it remains low until the end of the simulation. In the patterns of the various signals shown in Figures 6a and 6b, inertial oscillations are clearly visible. SSH time series were subsampled every 17 h to filter inertial oscillations which showed an amplitude of 2 cm in the first day. However, it is unlikely that these oscillations markedly affected the results of our simulations.

3.2.3. Homogenous Case

[54] A simulation (BCh; see Table 1) in homogenous temperature conditions with the same wind conditions as in the BC simulation was performed to characterize the role of stratification in the development of a poleward jet.

[55] Figure 6b shows the longshore maximum velocities on the shelf for the homogenous case at the 2°W, 44.5°N and 46.5°N transects. On day 1, velocities along the Spanish coast in the homogenous case and in the BC simulation are the same. Velocities in the homogenous case stay constant at about 60 cm s^{-1}, while BC velocities continue to grow because of the set of baroclinic currents. Along the French coast, at latitudes 44.5°N and 46.5°N, maximum velocities in the homogenous case are weak compared to the BC; they reach their maximum after 3 d and then decrease after the wind stops and vanish 2 d later. Patterns observed for the velocities in the BC do not occur in the homogenous case.

[56] In the homogenous case, the SSH at latitude 44.5°N (Figure 6c) is close to the SSH in the BC on the first day. The SSH then stays rather constant until the wind stops blowing, while in the BC it continues to grow until the wind stops. Velocities along the French coast do not exceed 15 cm s^{-1} and quickly decrease when the wind stops.

3.2.4. Comparison With Observations

[57] The BC simulation done with schematic conditions (bathymetry, stratification, wind) reproduced the main characteristics of the poleward jets observed nearshore based on ADCP measurements. The downwelling circulation on the French coast highlighted in observations is well reproduced. For example, the development of a strong poleward current (up to 20 cm s^{-1}) occurs after 2 d of 10 m s^{-1} westerlies. The vertical structures of the current are similar, with a rather homogeneous surface layer and a decrease toward the bottom. Orders of magnitude of currents are also similar, currents in simulations are stronger in the BC (up to 50 cm s^{-1}) than in observations (up to 32 cm s^{-1} in 2008 and 24 cm s^{-1} in 2009) that were done on one point, not necessarily at the location of the strongest current. These differences can be explained by the fact that, in the BC, westerlies blew stronger and longer than in observations. The stronger stratification imposed in the BC compared to the stratification observed offshore in summer 2008 may also play a role in the velocity differences noted between simulations and observations. The width of the jet, which appears limited to about 50 km in simulations, is in accordance with observations, which show that it is restricted to depths of less than 100 m. Associated with this current, bottom temperatures rise quickly along the coastal strip swept by the offshore displacement of the bottom front, in simulations and in observations alike.

[58] An important feature of the generated poleward current is its persistence. In 2008, 2 d of westerlies led to 8 d of intense poleward currents and probably more since the record stops before the end of the event. In 2009, 3 d of westerlies led to 22 d of poleward currents, even though the winds that followed the event were light southward upwelling favorable winds. Simulations show that after 15 d, poleward currents that occur in stratified conditions do not decrease but appear rather constant with velocities of the order of 5–10 cm s^{-1}, which are values similar to those that were observed.

[59] There is one main discrepancy between observations and simulations. Measurements show that poleward currents started before the increase in bottom temperature, which contradicts the supposed triggering mechanism. This discrepancy can be attributed to the fact that the ADCP was located at 54 m depth in 2008 and 51 m in 2009 and was not at the initial location of the front (where currents are maximum according to the thermal wind balance), which was probably closer to shore. Before the ADCP can measure an increase in bottom temperature, the front must drop from its initial position to the depth of the ADCP.

3.3. Longshore Evolution of Poleward Currents

[60] Velocities along both coasts are studied more in detail for the BC experiment and for two other experiments: weaker stratification (surface layer of 10 m, run 40; see Table 1) and longer wind duration (6 d, run 26; see Table 1). Results are presented in Figure 7. The maximum barotropic velocities along the Spanish coast (on the cross-shore transect) (6°W to 2°W) and the French coast (43.8°N to 48°N) are shown in Figures 7a and 7b, respectively. Along the Spanish coast, velocities increase very quickly. There is an east-west gradient of intensity: at 6°W, the maximum velocity is about 30 cm s^{-1} just before the wind stops, whereas it reaches 45 cm s^{-1} at 2°W. This indicates a cumulative effect in the longshore direction. When the wind stops, the velocities decrease quickly eastward and vanish within one week on the eastern side of the Spanish coast.

[61] Along the French coast, the situation is fairly different and circulation sets up because of propagative processes. Two main processes that propagate poleward currents were clearly identified with two branches of intense velocities. In the very first days, poleward velocities increase quickly to the south and are triggered later in the north. The speed of "propagation," calculated as the speed necessary for velocity to reach 5 cm s^{-1} between latitude 44.7°N and latitude 47°N, is about 3.8 m s^{-1} (slope coefficient of the first black line in Figure 7b). This is the typical order of magnitude of a coastal trapped wave (CTW) as described by *Chapman* [1987]. More recently, *Pringle and Dever* [2009] describe this type of transient wave when upwelling relaxation causes poleward jets to develop along the Californian coast.

[62] In the north (north of latitude 45.4°N), a second maximum can be observed in accordance with maximum velocities shown in Figure 6b at 46.5°N. This second maximum depends on latitude; the speed of propagation of the maximum (calculated as the speed necessary for the velocity to reach 20 cm s^{-1}, slope coefficient of the second black line in Figure 7b) is about 73 cm s^{-1}. This propagation is close to

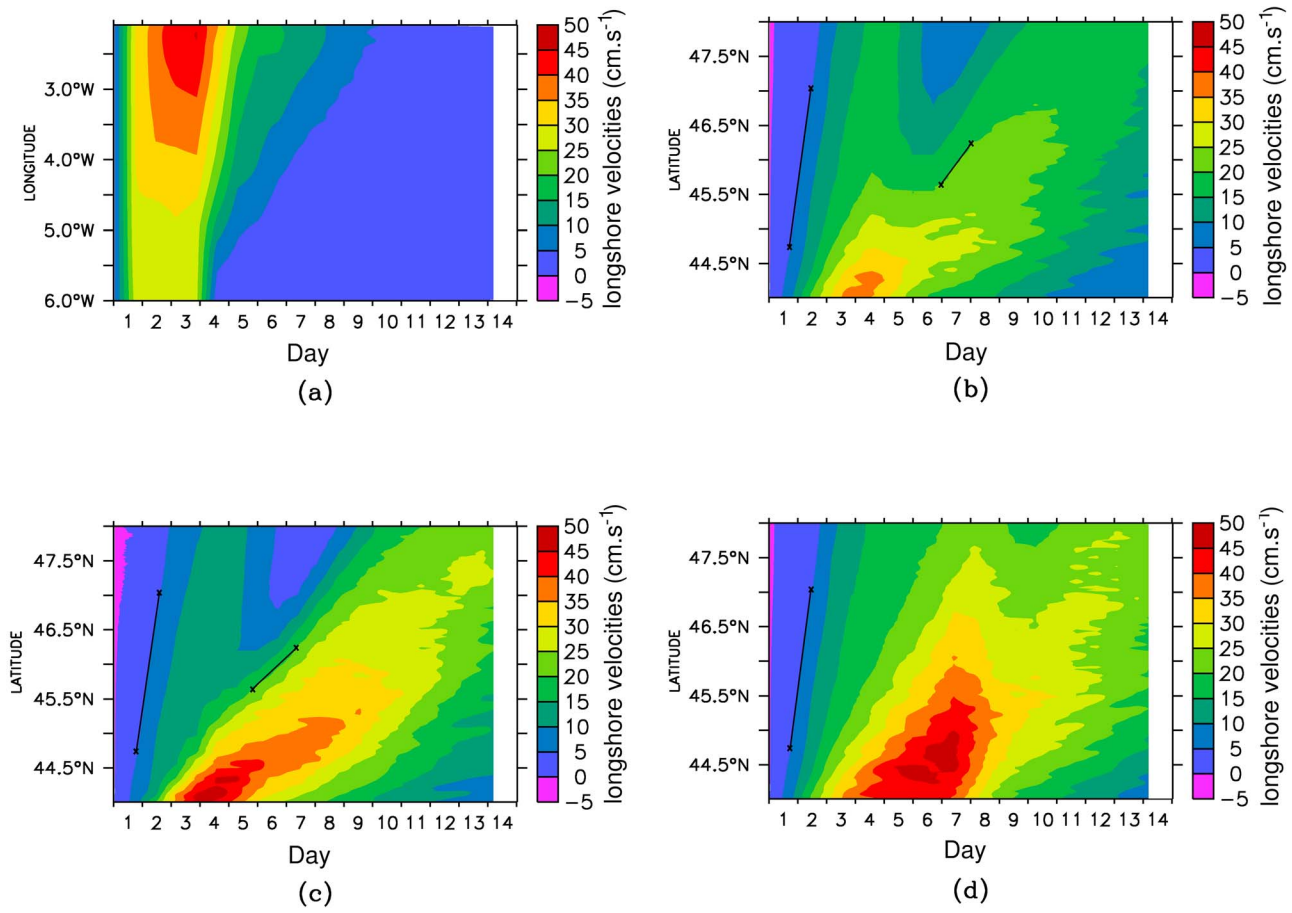

Figure 7. Maximum barotropic velocities over the shelf along (a) the Spanish coast in the BC simulation, (b) the French coast in the BC simulation, (c) the French coast in run 40 (thinner stratification), and (d) the French coast in run 26 (6 d of westerlies).

the speed of a linear inviscid internal Kelvin wave, i.e., $c = \sqrt{g'h}$, where g' is the reduced gravity $g' = g\Delta\rho/\rho_0$ and h is the thickness of the surface layer. In the BC simulation (22°C and 12°C for the surface and bottom layer temperatures), the value of g' is 0.02 m s^{-2} and h is 30 m, giving a c value of 77 cm s^{-1}. It can be then inferred that this propagation reflects the presence of an internal Kelvin wave propagating along the French coast after a high-speed CTW. The experiment with a surface layer of 10 m confirms these results (Figure 7c). The rapid development of the poleward current is very similar to the BC simulation (about 3.7 m s^{-1}, slope coefficient of the first black line in Figure 7c), but the second increase occurs more slowly at 51 cm s^{-1} (slope coefficient of the second black line in Figure 7c). This result is in agreement with inviscid theory, which gives a c value of 44 cm s^{-1} for an h value of 10 m. Velocities in the first increase were higher in the BC simulation; however, currents in the south and in the second increase were higher in the simulation with the smaller surface layer.

[63] In the BC simulation, the first process is stopped abruptly when the wind stopped blowing on day 3. Figure 7d shows the barotropic velocities of a simulation with 6 d of westerlies. Velocities were generally much higher than in the BC simulation. The first process was longer and stronger since the wind blows longer (its speed of propagation was the same as in the BC simulation, slope coefficient of the black line in Figure 7d). The minimum observed in the BC between the fast process and the slower one between days 5 and 7 north of 46.5°N is then shorter and less clear in this simulation.

3.4. Evolution of Bottom Temperature

[64] The change in bottom temperature is studied in the BC simulation. Figure 8a shows the change in temperature on a straight west-east transect along the Spanish coast at the bottom (depth, 46 m) along 43.4°N from 6°W to 2°W. Figure 8b shows the temperature on a straight north-south transect along the French coast at the bottom (depth, 46 m) along 1.1°W from 44°N to 48°N.

[65] The 17°C isotherm deepens along the Spanish coast (Figure 8a) at the same time as bottom temperatures change and when the wind stops, bottom temperatures at 46 m (18 km from the coast) reach the surface temperature because of the downwelling movement. Relaxation to initial temperatures highlights the presence of a wave that propagates at the same speed as a Kelvin baroclinic wave. At the end of the simulation, bottom temperature at 2°W is still at 16°C.

[66] Along the French coast (Figure 8b), temperatures increase quickly to 16°C in the south and this temperature

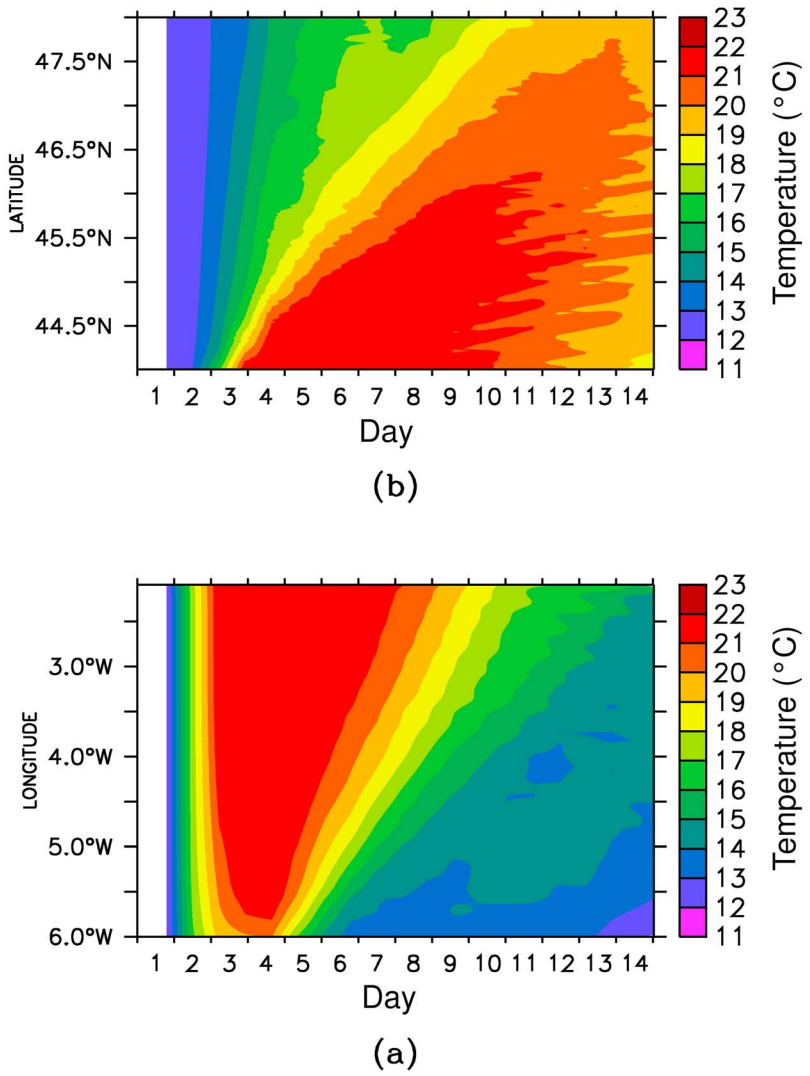

Figure 8. Bottom temperatures at 46 m depth (a) along the Spanish coast on the 43.4°N transect from 6°W to 2°W and (b) on the French coast on the 1.1°W transect from 44°N to 48°N.

increase is very quickly propagated northward. This temperature increase corroborates the first increase in velocities observed above. The very high propagation speed proves that the high bottom temperatures along the French coast were not primarily due to horizontal advection of warm water from the south, but to the deepening of the thermocline at the coast induced by local downwelling. South of 45°N, the temperature at the bottom rises quickly to 22°C. North of 46.5°N, after the first increase, temperatures remain at 17°C during the minimum velocities observed in the BC between the fast process and the slower one between days 5 and 7. The temperature at the bottom rises again, reaching 21°C when the second maximum of poleward velocities occurs. Between 45°N and 46.5°N, the increase in temperature is slower than south of 45°N, but steady and continuous. After 8 d, fluctuations at the bottom are still visible in the temperature signal. These instabilities are similar to those observed by *Allen and Newberger* [1996]; however, our horizontal scale is about 17 km greater than those they observed, which were between 2 and 4 km.

3.5. Assessment of the Main Forcing Mechanisms Along the French Coast

[67] To understand the mechanism that deepens the pycnocline along the French coast and gives rise to the poleward jets, three different simulations with the straight coastline bathymetry were performed. The first one aimed to study the direct effect of westerlies on the French coast disregarding any connection with the Spanish shelf. The aim of the two other simulations was to study the effect of different forcing taken from the BC simulation (density and SSH) and to understand which parameters control the observed poleward jets that were modeled along the French coast.

3.5.1. Effect of a Local Cross-Shore Wind Along a Straight Coast: Run SC1

[68] SSH was set to zero at open boundaries (south, north and west), temperature was also forced to its initial condition at open boundaries. Results are briefly commented below because, as expected, they do not show any significant increase in bottom temperatures or intense poleward jets observed during both measurement periods and in the BC

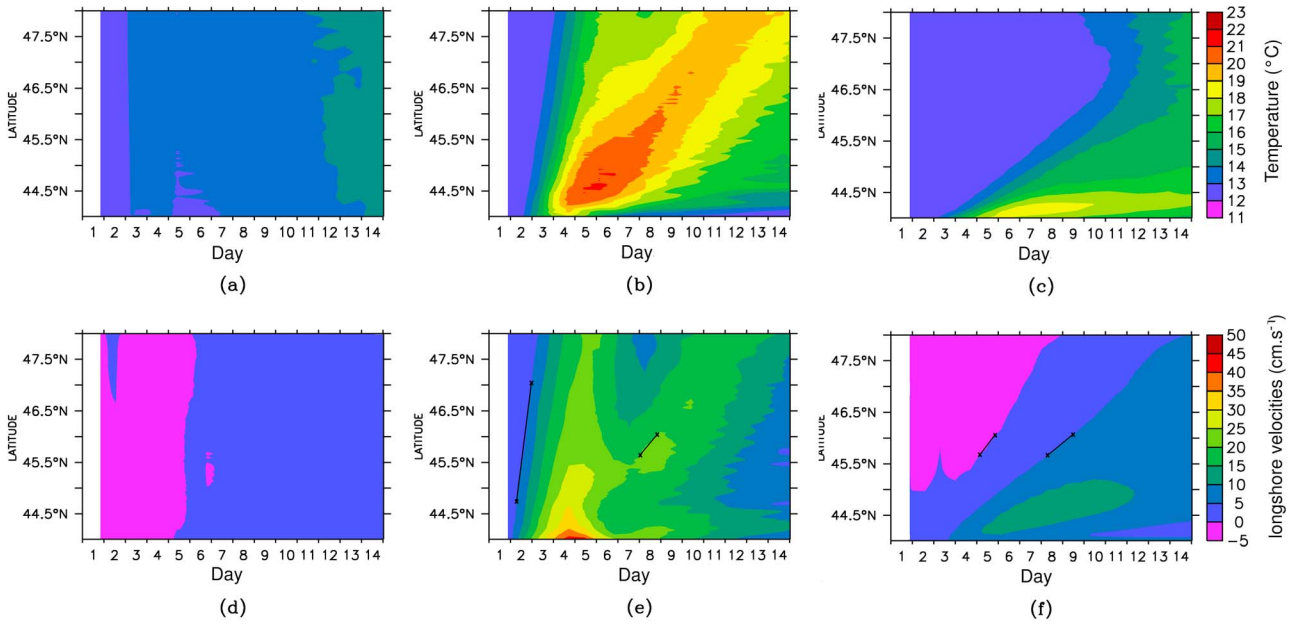

Figure 9. Bottom temperatures along the French coast on the 1.1°W transect from 44°N to 48°N at 46 m depth for (a) run SC1, (b) run SC2, and (c) run SC3. Maximum barotropic velocities over the shelf along the French coast for (d) run SC1, (e) run SC2, and (f) run SC3.

simulation (Figures 9a and 9d). The effect on temperature is very weak. As expected, barotropic velocities are southward. After 1 h of simulation, the SSH increases to a maximum of 3.7 cm along the French coast. After 9 h, a weak poleward jet of about 8 cm s^{-1} is observed at the location of the front all along the coast and persists until the end of the westerlies. This jet is linked to a weak deepening of the bottom front, about 2 m after 24 h of westerlies. Surface currents pushed by westerlies are southward in the surface Ekman layer. Cross-shore circulation in the homogeneous surface layer developed with onshore currents on the surface and offshore currents at the bottom of the surface layer. Cross-shore currents under the surface layer are also offshore but weaker. After 3 d of westerlies, poleward currents remain low compared to those observed in the BC, the maximum longshore poleward velocities are about 8 cm s^{-1} just before the winds stop and decrease later on. From this simulation, it can be inferred that cross-shore wind stress blowing on a straight coastline is not the main cause of the poleward jet observed.

3.5.2. Forcing on the South Boundary Based on Conditions Extracted From the BC: Runs SC2 and SC3

[69] The aim of this simulation was to understand the circulation observed in the BC simulation along the French coast. The straight coastline bathymetry was used. Southern boundary conditions were forced with results extracted from the BC simulation at the same 43.9°N latitude to understand how the setup induced by the downwelling circulation along the Spanish coast can affect circulation along the French coast. No wind was imposed in these simulations, the ocean is at rest at the beginning of the simulations and the forcing is only set on the southern boundary conditions.

[70] In the SC2 run, the current in open boundary conditions is simply a null longshore gradient of velocities and the temperature is forced to its initial value during the whole simulation. This simulation, where only SSH was forced, reproduces very similar velocity patterns as those observed in the BC simulation (compare Figure 9e with Figure 9b). The two increases in velocity are still identified; the fast one propagates at 4.2 m s^{-1} (slope coefficient of the first black line in Figure 9e) and 0.65 cm s^{-1} for the slower one (slope coefficient of the second black line in Figure 9e). Bottom temperature increases are similar to those observed in the BC simulation (compare Figure 9b with Figure 8b). The main difference is that temperatures weaken in the south on day 7 after the second rise of velocities whereas they remain warm in the BC simulation.

[71] In run SC3, only the density structure extracted from the BC simulation was forced on the south boundary. The fast increase in bottom temperature that occurred when SSH is forced (run SC2) disappears. A temperature increase propagates slowly to the north up to 19°C at the bottom (Figure 9c). The deepening of the front at the forced south boundary propagates to the north. It is accompanied by a rise in barotropic velocities to 15 cm s^{-1} which also slowly propagate to the north (Figure 9f). The propagation velocity (calculated as the speed necessary for the velocity to reach 5 cm s^{-1}, slope coefficient of the first black line in Figure 9f) is about 73 cm s^{-1} and about 44 cm s^{-1} if the propagation speed is calculated as the speed necessary for the velocity to reach 10 cm s^{-1} (slope coefficient of the second black line in Figure 9f). These temperature increases are the result of the deepening of the imposed front, creating cross-shore density gradients. These warm waters (Figure 9c) correspond to the differences in the south after day 7 between the change in temperature in the BC (Figure 8b) and the change in temperature in the SC2 run (Figure 9b) where temperatures decrease. This shows that the warm waters in the south after day 7 result from the downwelling along the Spanish coast and horizontal advection in the corner of the Bay of Biscay.

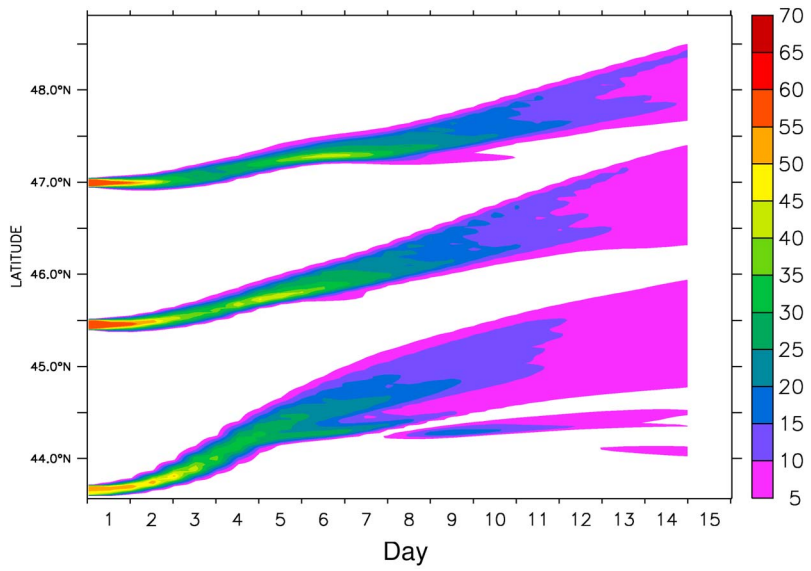

Figure 10. Depth-averaged concentration as a function of latitude and time along 1.14°W. Substances are initialized on the shelf at latitudes 44°N, 45°N, 46°N, and 47°N.

3.6. Effect on Transport

[72] To evaluate the distance over which waters are transported, a generic substance was initialized (at the value of 1) in the BC simulation on the French shelf of the Bay of Biscay on three strips centered on latitudes 43.65°N, 45.4°N and 47°N. Strips have a longitudinal width of 12 km and spread across the entire shelf width; the substance is initialized over the entire water column at each grid cell. Figure 10 shows the maximum value of the substance on the shelf (from longitude 1.25°W to 1.15°W, which is the approximate location of the jet) over time. Advection is all the more important when the substance is initialized in the southern part of the modeled domain. The poleward propagation occurs first for the substance initialized in the south and then is delayed in the north. At 47°N, poleward advection occurs in two steps. Advection first occurs from day 2 to 5 and then almost completely stops on day 5. Then it resumes from day 6 to the end of the simulation. These two separate advection periods highlight the occurrence of the two processes described above in section 3.3. For the substance initialized at 43.65°N and 45.4°N, advection is continuous. The highest poleward velocity is reached by the substance initialized at 43.65°N and is about 34 cm s^{-1} (calculated between days 4 and 5).

[73] After 4 d, the substance initialized at 43.65°N is transported north over 104 km (latitude 44.6°N), after 6 d over 160 km (latitude 45.1°N) and after 9 d over 225 km (latitude 45.7°N) (these calculations were made with a threshold detection of the sum of the substance over the water column of 1).

4. Discussion

4.1. Dynamical Interpretation

[74] The Mars3D model was used to understand the mechanism of the observed poleward currents. Different processes involved in the response to westerlies along the French and Spanish coasts could then be identified.

[75] The direct effect of cross-shore winds along the French coast is quite weak; it was studied in the SC1 simulation. The front deepens by about 1 m and creates weak longshore currents of about 8 cm s^{-1} at the front, below the surface layer. Surface longshore currents are driven southward by Ekman transport. These results are very similar to a previous experiment by *Tilburg* [2003]. The direct response of cross-shore winds along the French coast explains only part of the generation of poleward currents; it is a relatively minor process that cannot explain the strength of the observed current.

[76] The main features of the circulation along the French coast are very similar to the circulation induced by an longshore pressure gradient over a stratified shelf as described by *Chapman and Lentz* [2005], who showed that an external longshore pressure gradient is able to generate poleward flow and downwelling. Although the mechanism that generates these longshore pressure gradients were not assessed in detail, we showed that, in the Bay of Biscay, westerlies lead to an increase in SSH on the Spanish coast, particularly in the southeastern area (Figures 5a, 5d, 5g, 5j, and 5m). The increase in SSH induces an longshore pressure gradient that propagates along the French shelf. The propagation of the SSH gradient is associated with the development of a poleward flow on the French shelf. The bottom Ekman transport induces downslope bottom currents which advect lighter coastal waters offshore (not shown). This buoyancy advection deepens the front, generating horizontal density gradients in the bottom boundary layer, associated with a poleward jet according to the thermal wind balance. The generation of the first jet observed in the BC is due to a local downwelling-induced circulation.

[77] In a series of papers, *Austin and Lentz* [2002], *Chapman* [1987] and *Chapman and Lentz* [2005] describe the main characteristics of circulation induced by winds and/or longshore gradients over a stratified shelf with 2DV models that ignore the longshore dimension. Therefore, these papers were not able to discuss the transient

mechanisms that resemble CTWs that propagate poleward (leaving the coast to the right). We demonstrated here that two types of wave are generated: high-speed propagative waves of about 3–4 m s^{-1}, as observed by *Pringle and Dever* [2009] in their models of upwelling relaxation, and the leading edge of a baroclinic Kelvin waves whose velocities do not reach 1 m s^{-1}.

[78] The generation of the second slower wave is due to north-south density gradients, as clearly demonstrated in the SC3 run (Figures 9c and 9f) where the deepening of the front simulated in the BC simulation was forced at the Southern boundary. In the SC2 run (only SSH imposed at the southern boundary), even if the density field is not forced, a poleward propagating wave nevertheless occurs (Figure 9e). This can be explained by the fact that the external longshore pressure gradient generated by the westerlies is not uniform across the shelf. The gradient is much greater near the Spanish coast and thus the poleward flow and the induced downwelling described above are stronger on the southern part of the Aquitaine shelf than on the northern part. As a result, the front is deeper in the south which also creates north-south density gradients and initiates a baroclinic Kelvin wave that propagates poleward.

[79] The persistence of the current more than one week after the wind stops in stratified conditions is an important feature. In contrast, in homogeneous conditions, longshore currents decrease quickly and disappear after nearly 3 d as shown in Figure 6b. The role of stratification in decreasing the bottom stress over the shelf has been studied in detail by *Chapman* [2002] and *Chapman and Lentz* [2005]. Without considering the forcing of the current, they show that the decrease in a poleward current along a sloping shelf depends on both frictional spin down and buoyancy shutdown. Both phenomena occur on different time scales, depending mainly on a frictional parameter and stratification through the Brunt-Vaissala frequency and bottom slope. Without stratification, frictional spin down occurs solely on a time scale of $h.r^{-1}$ (h: water depth, r: linear bottom friction coefficient). Considering a typical r value of 2.5 e^{-4}m s^{-1} and a mean height of 60 m, the *e*-folding time is about 2.6 d, which is consistent with our model results for the homogeneous situation (see BCh on Figure 6b). When there is stratification, the estimated buoyancy shutdown time scale has been given by *Garrett et al.* [1993] and its role relative to the frictional spin down has been assessed by *Chapman* [2002]. Application of these studies to realistic or schematic case is not straightforward, but *Chapman* [2002] indicates that buoyancy shutdown could be important on time scales greater than 5 d for conditions typically observed over shelves.

[80] In support of the hypothesis of buoyancy spin down, the longshore bottom velocity in 2009 weakened dramatically 4 d after the birth of the jet. Over the next two weeks, although the main current decreased from 10 to 5 cm s^{-1}, the bottom velocity was always less than 1 cm s^{-1} (Figure 4d), the weakest values during the whole deployment. This is also visible for the BC simulation in Figures 5b and 5c. As a result, bottom stress becomes very weak and could favor the persistence of the poleward jet event under moderate upwelling favorable conditions.

[81] The downwelling along the Spanish coast triggers the poleward currents along the French coast. Thus, winds along the Spanish coast must be downwelling favorable. The event of west-southwesterly winds from 5 to 7 June 2009 did not trigger a poleward jet. These west-southwesterly winds were calculated near the location of the ADCP at 44.5°N, 2°W. However, winds analyzed along the Spanish coast at 43.5°N, 3°W show a different pattern (Figure 2). Westerlies were weaker and not continuous (westerly component from 7 to 9 m s^{-1} 12 h on 5 June and a gust of 8.1 m s^{-1} on 7 June). Thus, westerlies did not blow enough to trigger downwelling along the Spanish coast and, consequently, the poleward jet along the French coast did not occur. During the two other major events of westerlies that did trigger poleward jet winds along the Spanish coast at (43.5°N, 3°W), winds were similar in terms of duration and intensity along the French coast at (44.5°N, 2°W). This shows that the currents observed near the Arcachon Bay can depend on the winds that blow 120 km south, along the Spanish coast.

4.2. Sensitivity Analysis

[82] Several simulations were performed to vary the basic parameters of the system in order to test their role in circulation and hydrology and to determine in which conditions of wind and stratification the poleward jet could appear. The magnitude of the wind, its duration, the depth of stratification, the surface temperature and the direction of the wind were made to vary. The schematic right angle coastline bathymetry representative of the Bay of Biscay was used.

4.2.1. Simulations for Different Wind Directions

[83] The flow on the shelf along latitude 44.5°N integrated over the first 100 h of simulations for different wind orientations is shown in Figure 11a. Initial temperatures and salinities are the same as in the BC simulation. Westerlies and easterlies are the winds that result in the most important flow. Surprisingly, flow obtained under northerlies and southerlies are close to zero because of counter currents. The maximum along-shelf velocities on the shelf at latitude 44.5°N after 3 d of simulation (just before the wind ceases) are shown in Figure 11b. The most important poleward speed and flow are reached with winds from the west and the southwest. These results confirm the usefulness of studying westerlies more in detail, because westerlies are frequent in this area.

[84] Simulation with northwesterly winds shows, as in the BC simulation, a rise in SSH in the southeastern area of the bay, but a decrease along the French coast because of the upwelling favorable winds. Downwelling, as observed in the BC simulation along the French coast, does not occur because upwelling has developed along the French coast. Once the wind stops, the upwelling weakens and the warm waters from Spain can propagate along the coast.

[85] Simulation with the southwesterly winds differs. Southwesterly winds are downwelling favorable along both coasts giving rise rapidly to downwelling jets on both coasts. As a result, the propagation of the internal Kelvin wave observed along the French coast in the BC simulation does not occur in this simulation.

4.2.2. Influence of Stratification

[86] The initial potential energy (IPE) anomaly is compared to the flow in the simulations with different density profiles. IPE was calculated as in equation 1: the integral

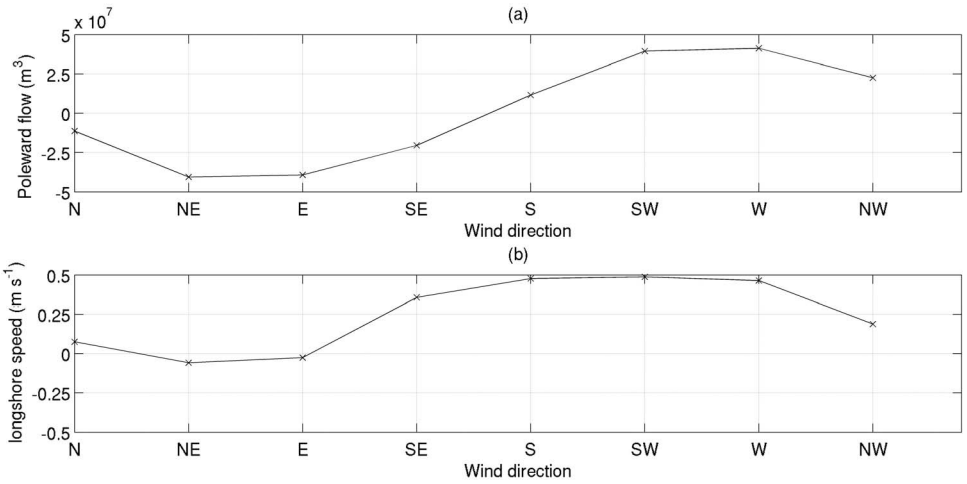

Figure 11. (a) Flow integrated over 100 h of simulations on the 44.5°N transect for simulations with different wind directions and (b) maximum along-shelf depth-averaged velocities on the 44.5°N transect after 72 h for simulations with different wind directions.

over the depth of the difference between the initial density in the profile and the mean initial density over the profile. This integral was done on a profile of 160 m, the maximum depth on the shelf.

$$PE = \frac{1}{H}\int_{H}^{0} g(\rho(z) - \bar{\rho})zdz \qquad (1)$$

[87] The integrated baroclinic flow on the shelf (the barotropic flow from the homogenous simulation was removed), at latitude 44.5°N for various initial density profiles and forcing parameters was calculated. It is shown in Figure 12, calculated 12 h after the wind stopped as a function of the square root of the IPE of the profile for various temperature (runs 27 to 38, see Table 1) and various depth of the homogenous surface layer (runs 39 to 44, see Table 1). Results from six additional simulations are also shown (runs 45 to 51, see Table 1). The temperature and salinities in the simulation were initialized with mean profiles on the Aquitaine shelf extracted from the monthly climatology Bobyclim (http://www.ifremer.fr/climatologie-gascogne) corresponding to realistic density situations (in terms of salinity and temperature) in February, April, June, August, October and December (profiles are given in Figure 13).

[88] Flow and the square root of IPE are shown for simulations 27 to 38 in which surface temperature was varied (Figure 12). The weakest values of flow and square root of IPE correspond to the weakest surface temperatures. This curve shows that the flow depends linearly on the square root of IPE. The values for the simulations 39 to 44 with different surface layer thicknesses are also shown. The weakest values correspond to the thickest surface layer. The results from the simulations 45 to 51 initialized with density values taken from the climatology model are represented by dots of different colors. This shows that the rate of transformation from potential energy to kinetic energy (proportional to the square of velocity) is nearly constant.

[89] Results from the seasonal profiles demonstrate that during winter and spring, the flow remains low, indicating that the jet is weak or was not triggered because density differences are not strong enough. The month that leads to the greatest flows is August, however June and October flows show large flows as well.

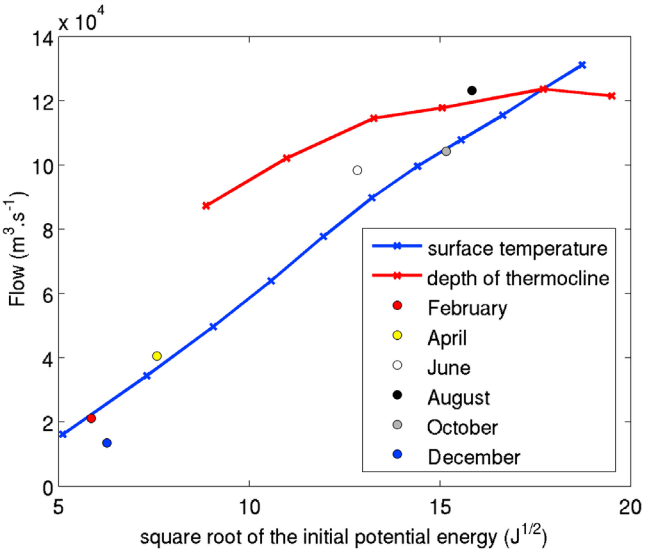

Figure 12. Flow calculated 12 h after the wind stops (i.e., day 3.5) on the 44.5°N transect as a function of the square root of the initial potential energy for the first parameter (temperature of the surface layer, blue line) and for the second parameter (depth of the homogenous surface layer, red line). Colored dots give the results from six additional simulations corresponding to realistic density situations (in terms of salinity and temperature) on the Aquitaine shelf in February, April, June, August, October, and December; density profiles extracted from the monthly Bobyclim climatology.

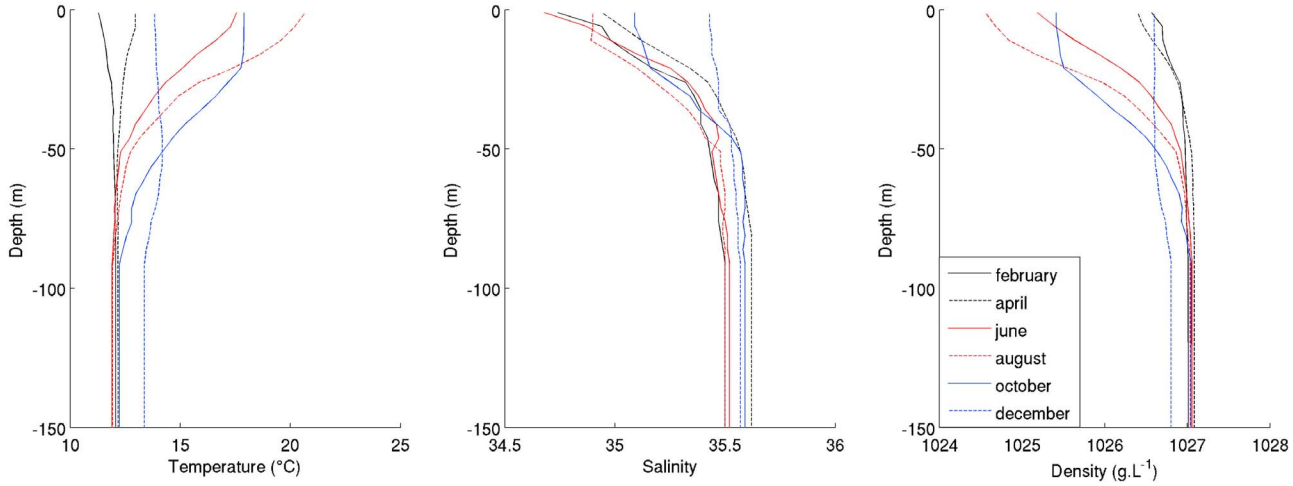

Figure 13. Profiles of temperature, salinity, and density for the various realistic stratifications averaged on the Aquitaine shelf (from 43.4°N to 44.6°N and 2.2°W to 1°W) extracted from the monthly Bobyclim climatology.

[90] These results are valid for winds of 3 d and 10 m s^{-1}. Additional runs were conducted to study the impact of the intensity and duration of winds.

[91] A complete budget study is beyond the scope of this paper and was not carried out. Our objective was to demonstrate that fluxes in the poleward jet depend mainly on initial stratification and that westerlies can be considered as the triggering mechanism that creates bottom fronts and moves them offshore and poleward (through CTWs). The remaining circulation after the winds cease apparently depends only on the stratification conditions as shown in Figure 12 (for the same duration of winds). Several simulations (not shown) examined the shelf response to different wind speeds and durations and results show that the linear dependence of the maximum flux on the square root of IPE remains valid.

[92] Simulations in which stratification is made to vary (depth of stratification and temperature of the surface layer) reveal the importance of stratification in triggering jets. Accordingly, without stratification, currents remain low on the French shelf. Tests on the depth of the thermocline show that even small thermoclines can lead to strong flow. On the other hand, tests on surface temperature reveal that the intensity of the jet depends strongly on the temperature gradient.

[93] Finally, even weak stratification in terms of depth and density gradients can have a strong impact along the French coast and thus the jet can be triggered whenever the thermal stratification can be set up, i.e., from late spring to late autumn.

4.2.3. Influence of Magnitude and Duration of the Wind

[94] Simulations that vary the magnitude (runs 14 to 21, see Table 1) and the duration of the wind (runs 22 to 26, see Table 1) show that weak westerlies of 6 m s^{-1} for 3 d as well as strong westerlies (of 10 m s^{-1}) for 2 d are able to generate intense poleward jets along the French coast with maximum velocities about 15 and 25 cm s^{-1} (on the 44.5°N transect), respectively, as long as stratification is present. These simulations show that flow depends linearly on the duration of the wind and wind stress.

5. Summary

[95] We showed that schematic simulations are able to reproduce the main features of the observations recorded during two hydrodynamic surveys. The triggering mechanism of the transient poleward current is unequivocally due to the propagation of a downwelling circulation induced along the Spanish coast to the French coast. This circulation generally appears to be independent of past wind patterns, spatial variation in wind stress or longshore bathymetry gradients along the French coast. Even though these three conditions are not perfectly met in the field (e.g., persistent, albeit weak, past wind patterns, irregular coastline and irregular shelf width), they probably only have a weak influence on circulation patterns.

[96] This study was inspired by recent unexpected observations of poleward currents. The processes described in this study are barely visible in classical and operational observatory systems. Downwelling has no signature in sea surface temperatures (SST) and are invisible in satellite SST monitoring. The associated sea surface variations are weak and hardly measurable. This may explain in part why this phenomenon has gone unobserved thus far. New monitoring programs must be set up using, for example, high-frequency radar to measure surface currents or incorporate regular sea bottom temperature measurements.

[97] These jets can have a strong impact on the ecosystem for various reasons. These currents are suspected to transport toxic water masses from the Basque Country, where an important source of toxic phytoplankton (i.e., *Dinophysis*) has been identified [*Batifoulier et al.*, 2011]. The transport simulated in Figure 10 shows that this trajectory is realistic: after 4 d, the substance initialized at latitude 43.65°N (area where *Dinophysis* is suspected to grow) was advected offshore from Arcachon Bay. Tidal pumping of the Archon Bay is then able to transport *Dinophysis* into the bay itself.

[98] In future investigations, more realistic bathymetry conditions need to be used to better reflect the actual contours of the coastline. The model could be enhanced in three ways. First, the coastline is not straight and has some bathymetry irregularities. Second, the French coast is not perfectly straight: it inclines at 8° (trigonometrically positive) compared to a straight north-south axis and westerlies may then have a weak downwelling favorable component. Finally, the impact of the Capbreton canyon on the propagation of the different processes over the French shelf is unknown. Future models will help estimate how far these currents propagate and study the possible connection with the autumnal currents on the Armorican shelf described by *Lazure et al.* [2008].

[99] **Acknowledgments.** The authors would like to thank the personnel of the REPHY program (IFREMER LER Arcachon), the EPOC staff (Natalie Bonneton, Stephane Bujan, Beatrice Bec, Gaelle Pauliac, and Guillaume Detandt), and the Côte d'Aquitaine crew for the organization and participation in the ARCADINO surveys. We acknowledge Guillaume Charria for his help on buoy processing. We also thank the LOCEAN laboratory which provided one of the buoy trajectories we used in this study (GLOSCAL project, funded by the CNES). This work was funded by the European Union with FEDER funds and by IFREMER. This work is also a contribution to the EPIGRAM project, funded by CNRS (national program LEFE/IDAO) and ANR (grant ANR-08-BLAN-0330-01).

References

Allen, J. S., and P. A. Newberger (1996), Downwelling circulation on the Oregon continental shelf. Part I: Response to idealized forcing, *J. Phys. Oceanogr.*, *26*, 2011–2035, doi:10.1175/1520-0485(1996)026<2011:DCOTOC>2.0.CO;2.

Austin, J. A., and S. J. Lentz (2002), The inner shelf response to wind-driven upwelling and downwelling, *J. Phys. Oceanogr.*, *22*, 2171–2193.

Batifoulier, F., P. Lazure, L. Velo-Suarez, D. Maurer, P. Bonneton, C. Dupuy, and P. Gentien (2011), Distribution of *Dinophysis* species in the Bay of Biscay and possible transport pathways to Arcachon Bay, *J. Mar. Syst.*, doi:10.1016/j.jmarsys.2011.12.007, in press.

Chapman, D. C. (1987), Application of wind-forced, long, coastal-trapped wave theory along the California coast, *J. Geophys. Res.*, *92*, 1798–1816, doi:10.1029/JC092iC02p01798.

Chapman, D. C. (2002), Deceleration of a finite-width, stratified current over a sloping bottom: Frictional spindown or buoyancy shutdown?, *J. Phys. Oceanogr.*, *32*, 336–352, doi:10.1175/1520-0485(2002)032<0336:DOAFWS>2.0.CO;2.

Chapman, D. C., and S. J. Lentz (2005), Acceleration of a stratified current over a sloping bottom, driven by an alongshelf pressure gradient, *J. Phys. Oceanogr.*, *35*, 1305–1317, doi:10.1175/JPO2744.1.

Charria, G., P. Lazure, B. Le Cann, A. Serpette, G. Reverdin, S. Louazel, F. Batifoulier, F. Dumas, A. Pichon, and Y. Morel (2011), Surface layer circulation derived from Lagrangian drifters in the Bay of Biscay, *J. Mar. Syst.*, doi:10.1016/j.jmarsys.2011.09.015, in press.

Crépon, M., and C. Richez (1982), Transient upwelling generated by two-dimensional atmospheric forcing and variability in the coastline, *J. Phys. Oceanogr.*, *12*, 1437–1457, doi:10.1175/1520-0485(1982)012<1437:TUGBTD>2.0.CO;2.

Demerliac, M. A. (1974), Calcul du niveau moyen journalier, *Ann. Hydrogr.*, *5*, 49–57.

Ferrer, L., A. Fontán, J. Mader, G. Chust, M. González, and V. Valencia, Ad. Uriarte, and M. B. Collins (2009), Low-salinity plumes in the oceanic region of the Basque Country, *Cont. Shelf Res.*, *29*, 970–984, doi:10.1016/j.csr.2008.12.014.

Froidefond, J. M., P. Castaing, and J. M. Jouanneau (1996), Distribution of suspended matter in a coastal upwelling area. Satellite data and in situ measurements, *J. Mar. Syst.*, *8*(1–2), 91–105, doi:10.1016/0924-7963(95)00040-2.

Frouin, R., A. F. Fuiza, I. Ambar, and T. J. Boyd (1990), Observations of a poleward surface current off the coasts of Portugal and Spain during the winter, *J. Geophys. Res.*, *95*, 679–691, doi:10.1029/JC095iC01p00679.

Garrett, C., P. MacCready, and P. Rhines (1993), Boundary mixing and arrested Ekman layers: Rotating stratified flow near a sloping boundary, *Annu. Rev. Fluid Mech.*, *25*, 291–323, doi:10.1146/annurev.fl.25.010193.001451.

Garvine, R. W. (1987), Estuary plumes and fronts in shelf waters: A layer model, *J. Phys. Oceanogr.*, *17*, 1877–1896, doi:10.1175/1520-0485(1987)017<1877:EPAFIS>2.0.CO;2.

Gaspar, P., Y. Gregoris, and J. M. Lefevre (1990), A simple eddy kinetic energy model for simulations of the oceanic vertical mixing: Tests at station Papa and Long-Term Upper Ocean Study site, *J. Geophys. Res.*, *95*, 16,179–16,193, doi:10.1029/JC095iC09p16179.

Gill, A. E. (1982), *Atmosphere-Ocean Dynamics*, *Int. Geophys. Ser.*, vol. 30, 662 pp., Academic, New York.

Koutsikopoulos, C., and B. Le Cann (1996), Physical processes and hydrological structures related to the Bay of Biscay anchovy, *Sci. Mar.*, *60*, 9–19.

Lavin, A., L. Valdes, F. Sanchez, P. Abaunza, A. Forest, J. Boucher, P. Lazure, and A. M. Jegou (2006), The Bay of Biscay: The encountering of the ocean and the shelf, in *The Sea, Volume 14B: The Global Coastal Ocean: Interdisciplinary Regional Studies and Syntheses*, edited by A. P. Robinson and K. Brink, pp. 933–1001, Harvard Univ. Press, Cambridge, Mass.

Lazure, P., and F. Dumas (2008), An external-internal mode coupling for a 3D hydrodynamical model for applications at regional scale (MARS), *Adv. Water Resour.*, *31*(2), 233–250, doi:10.1016/j.advwatres.2007.06.010.

Lazure, P., F. Dumas, and C. Vrignaud (2008), Circulation on the Armorican shelf (Bay of Biscay) in autumn, *J. Mar. Syst.*, *72*, 218–237, doi:10.1016/j.jmarsys.2007.09.011.

Le Cann, B. (1990), Barotropic tidal dynamics of the bay of Biscay shelf: Observations, numerical modeling and physical interpretation, *Cont. Shelf Res.*, *10*(8), 723–758, doi:10.1016/0278-4343(90)90008-A.

Le Cann, B., and A. Serpette (2009), Intense warm and saline upper ocean inflow in the southern Bay of Biscay in autumn-winter 2006–2007, *Cont. Shelf Res.*, *29*(8), 1014–1025.

Melton, C., L. Washburn, and C. Gotschalk (2009), Wind relaxations and poleward flow events in a coastal upwelling system on the central California coast, *J. Geophys. Res.*, *114*, C11016, doi:10.1029/2009JC005397.

Petus, C., G. Chust, F. Gohin, D. Doxaran, J. M. Froidefond, and Y. Sagarminaga (2010), Estimating turbidity and total suspended matter in the Adour River plume (South Bay of Biscay) using MODIS 250-m imagery, *Cont. Shelf Res.*, *30*(5), 379–392, doi:10.1016/j.csr.2009.12.007.

Pingree, R. D., and B. Le Cann (1989), Celtic and Armorican slope and shelf residual currents, *Prog. Oceanogr.*, *23*, 303–338, doi:10.1016/0079-6611(89)90003-7.

Pingree, R. D., and B. Le Cann (1992), Three anticyclonic Slope Water Oceanic eDDIES (SWODDIES) in the southern bay of Biscay in 1990, *Deep Sea Res.*, *39*(7/8), 1147–1175.

Pringle, J. M., and E. P. Dever (2009), Dynamics of wind-driven upwelling and relaxation between Monterey Bay and Point Arena: Local-, regional-, and gyre-scale controls, *J. Geophys. Res.*, *114*, C07003, doi:10.1029/2008JC005016.

Puillat, I., P. Lazure, A. M. Jegou, L. Lampert, and P. I. Miller (2004), Hydrographical variability on the French continental shelf in the Bay of Biscay, during the 1990s, *Cont. Shelf Res.*, *24*(10), 1143–1163, doi:10.1016/j.csr.2004.02.008.

Relvas, P., E. D. Barton, J. Dubert, P. B. Oliveira, Á. Peliz, J. C. B. da Silva, and A. M. P. Santos (2007), Physical oceanography of the western Iberia ecosystem: Latest views and challenges, *Prog. Oceanogr.*, *74*, 149–173, doi:10.1016/j.pocean.2007.04.021.

Sanay, R., A. Yankovsky, and G. Voulgaris (2008), Inner shelf circulation patterns and nearshore flow reversal under downwelling and stratified conditions off a curved coastline, *J. Geophys. Res.*, *113*, C08050, doi:10.1029/2007JC004487.

Tilburg, C. E. (2003), Across-shelf transport on a continental shelf: Do across-shelf winds matter?, *J. Phys. Oceanogr.*, *33*, 2675–2688, doi:10.1175/1520-0485(2003)033<2675:ATOACS>2.0.CO;2.

Valencia, V., J. Franco, A. Borja, and A. Fontán (2004), Hydrography of the southeastern Bay of Biscay, in *Oceanography and Marine Environment of the Basque Country*, *Elsevier Oceanogr. Ser.*, vol. 70, edited by A. Borja and M. Collins, pp. 159–194, Elsevier, Amsterdam, doi:10.1016/S0422-9894(04)80045-X.

Yankovsky, A. E., and D. C. Chapman (1997), A simple theory for the fate of buoyant coastal discharges, *J. Phys. Oceanogr.*, *27*, 1386–1401, doi:10.1175/1520-0485(1997)027<1386:ASTFTF>2.0.CO;2.

F. Batifoulier and P. Lazure, IFREMER, Centre de Brest, B.P. 80, F-29280 Plouzané, France. (pascal.lazure@ifremer.fr)

P. Bonneton, UMR CNRS EPOC 5805, Université de Bordeaux I, F-33405 Talence, France.